2011-08-11

Expanding Lamina Emergent Mechanism (LEM) Capabilities: Spherical LEMs, LEM Joints, and LEM Applications

Samuel E. Wilding
Brigham Young University - Provo

Expanding Lamina Emergent Mechanism (LEM) Capabilities:

Spherical LEMs, LEM Joints, and LEM Applications

Samuel E. Wilding

A thesis submitted to the faculty of
Brigham Young University
in partial fulfillment of the requirements for the degree of

Master of Science

Larry L. Howell, Chair
Spencer P. Magleby
David T. Fullwood

Department of Mechanical Engineering

Brigham Young University

Thesis Completed July 2011

ABSTRACT

Expanding Lamina Emergent Mechanism (LEM) Capabilities:
Spherical LEMs, LEM Joints, and LEM Applications

Samuel E. Wilding
Department of Mechanical Engineering, BYU
Master of Science

Lamina Emergent Mechanisms (LEMs) are a class of compliant mechanisms that can be manufactured from sheet goods and possess motion out of the plane of fabrication. LEMs can be designed to perform sophisticated motions. This thesis expands LEM understanding and increases the ability to utilize them in applications by introducing the fundamentals of spherical LEMs, creating joints suitable for LEMs, and providing an example of a LEM application.

In this thesis, the fundamentals of spherical LEMs are developed. This includes classification of all possible spherical 4R LEMs and a discussion of the motion characteristics of the various mechanisms. The motion characteristics associated with spherical 4R LEMs are then used to predict the motion of spherical 6R LEMs and arrays of spherical LEMs. Multiple spherical LEM prototypes are shown and discussed.

A common difficulty of working with compliant mechanisms, especially LEMs, is creating suitable joints. There is often a trade off between flexibility in the desired direction of deflection, and stiffness in directions of undesired deflection. For this thesis, LEM joints that possess higher off-axis stiffness, especially in tension and compression, than previous designs were developed: the I-LET, the T-LET, and the IT-LET. Joint geometries were optimized and then modeled in commercial finite element analysis (FEA) software capable of nonlinear analysis. These models were used to predict the bending of tensile/compressive stiffnesses of the joints. As a benchmark, lamina emergent torsional (LET) joints were modeled and optimized for maximum tension and compression loading while maintaining the same bending stiffness as the joint being compared. Mechanisms that utilized the new joints were created and are briefly discussed. The use of these joints allows for minimized parasitic motion under tension and compression loads and expands the capability of LEM joints.

The Lens Lift™ was developed to demonstrate an application of LEMs. The Lens Lift™ is a LEM device that allows for easier and more sterile use of disposable contact lenses. It possesses a monolithic structure and can be fabricated using simple manufacturing processes. As the contact lens user opens the blister pack used to store the lens, the lens is lifted out of the pack and presented to the user. The user can then lift the lens with one touch and place it in the eye. A provisional patent has been filed for the device and the device currently being evaluated by a major contact lens manufacturer for further development.

Keywords: LEMs, compliant mechanisms, spherical mechanisms, LEM joints

ACKNOWLEDGMENTS

I express my gratitude to Dr. Larry Howell for his guidance, counsel and support. He is an example of academic achievement, fatherhood, and leadership, among other things. Dr. Magleby has also been a consistent source of counsel and advice.

I especially thank my wife Erica and my son Cohen. They have been supportive and very patient with me throughout my academic career. Also, thank you to my parents and and my parents-in-law for their assistance. I also thank my Father in Heaven for His comfort, direction, and the inspirations that He blessed me with.

Most of the students in the CMR lab contributed to this research in at least some way. Thanks especially to Holly Greenberg for her assistance with the Lens Lift™ and to Quinten Aten for his help with finite element modeling. I also gratefully acknowledge ITWFormex® for providing prototype materials, and Brigham Young University for their financial assistance.

This material is based upon work supported by the National Science Foundation under Grant No. CMMI-0800606. Any opinions, findings, and conclusions or recommendations expressed in this material are those of the author and do not necessarily reflect the views of the National Science Foundation.

TABLE OF CONTENTS

LIST OF TABLES

LIST OF FIGURES

CHAPTER 1. INTRODUCTION

1.1 Thesis Outline

Lamina emergent mechanisms (LEMs) offer the advantages of simple topology and compactness. A LEM is a compliant mechanical device that is fabricated from a planar material with motion out of the plane of fabrication [2]. LEMs can perform sophisticated motions despite the simplicity of their topology. However, LEM application is currently limited because of a lack of basic understanding of their fundamental behavior, the limited number of joints available for LEM motion and a lack of examples that illustrate their design. This thesis addresses these issues by developing the fundamentals of spherical LEMs, creating new LEM joints, and providing an example of LEM design.

Several applications of LEMs have been developed including disposable mechanisms, mechanism arrays, scaled mechanisms, and deployable mechanisms [3]. Many of these mechanisms are limited to planar motion. Chapter 2 of this thesis describes and establishes the fundamentals of spherical LEMs to further expand the capabilities of LEMs and develop LEMs capable of spatial motion. Spherical mechanisms are the simplest mechanisms capable of spatial motion [4]. By nature, spherical mechanisms are compact [5] and become additionally compact as LEMs. Basic spherical LEMs, such as spherical 4R linkages, will be developed as well as more advanced linkages and arrays [3], such as spherical 6R linkages and arrays formed by serially linking multiple 4R linkages. Multi-layer [6] spherical LEMs will also be discussed.

Another limit to the capabilities of LEMs is the availability of joint types. The lamina emergent torsional (LET) [7] joint has been widely used but additional options are needed. Chapter 3 describes the development of three new LEM joints. The Inverted LET (I-LET), the Tension LET (T-LET), and the Inverted Tension LET (IT-LET) were developed to bear tensile, compressive, and a combination of tensile and compressive loads, respectively, with minimal parasitic motion. The LET joint is used as a benchmark to compare stiffnesses in tension and compression. Using closed

form equations, the geometry of the new joints was optimized for minimum bending stiffness. For valuable comparison, LET joint geometry was optimized for maximum tensile/compressive stiffness, while maintaining the same bending stiffness as the joint used in the comparison. Finite element analysis (FEA) was used to determine the stiffnesses of each of the joints. These joint provide additional options for designers of LEMs and address the issue of parasitic motion under tension and compression loads.

Chapter 4 describes the design of the Lens Lift™as a case study for LEM application. The Lens Lift™ is a LEM device designed to be used with disposable contact lens blister packs. As the blister pack is opened, the device is actuated and the lens is lifted out of the blister pack and presented to the user, for more convenient and sanitary access. Since disposable contact lenses are a mass produced commodity, a LEM device like the Lens Lift™ is well suited for incorporation into the current manufacturing processes. Chapter 5 reviews the work and suggests potential areas of future research related to this thesis.

In summary, the objectives of this thesis are to first, describe the fundamentals of spherical LEMs, including arrays of spherical mechanisms, thus developing LEMs capable of spatial motion. Second, to introduce LEM joints that allow for reduced parasitic motion under tensile and compressive loading conditions. The third objective is to describe the development of the Lens Lift™.

1.1.1 Spherical LEMs

Much of the research in LEMs and their application has been limited to planar mechanisms, with a few examples given of spherical LEMS [2, 3, 8]. Spherical mechanisms differ from planar mechanisms in that instead of every point on a link being constrained to a move in a plane, with all motion parallel; every point on a link is constrained to move on the surface of a sphere, with all sphere centers being concentric. Also, the axis of each link of the mechanism passes through the sphere center. This is illustrated by the skeleton diagram in Figure 1.1. At any time throughout the motion of the mechanism, the joints axes always pass through the center of the sphere. Although often shown as such, the links of a spherical mechanism do not have to be curved. The links can be any desired shape as long as the joint axes pass through the sphere center. This leads to mechanisms that feature complex and non-intuitive motion. Spherical mechanisms can also be serially linked

together to form more advanced mechanisms [9]. Spherical LEMs linked in this way can be used to form LEM arrays.

It has been proposed that there are only 33 different spherical 4-bar mechanism types [1]. Further restrictions exist for spherical LEMS. The criteria established by Cervantes et al. [1] suggest that only 17 of the 33 types of spherical mechanisms can be LEMs. An example of a Spherical 4-bar LEM is shown in Figure 1.2. The mechanism lays flat in its initial position but exhibits complex out-of-plane motion when actuated. The criteria established by [1] will aid in the development the fundamentals and capabilities of spherical LEMs. Motion, size and shape restrictions, as well as what types of spherical mechanisms best fulfill certain tasks are all factors that will help define the fundamentals of spherical LEMs.

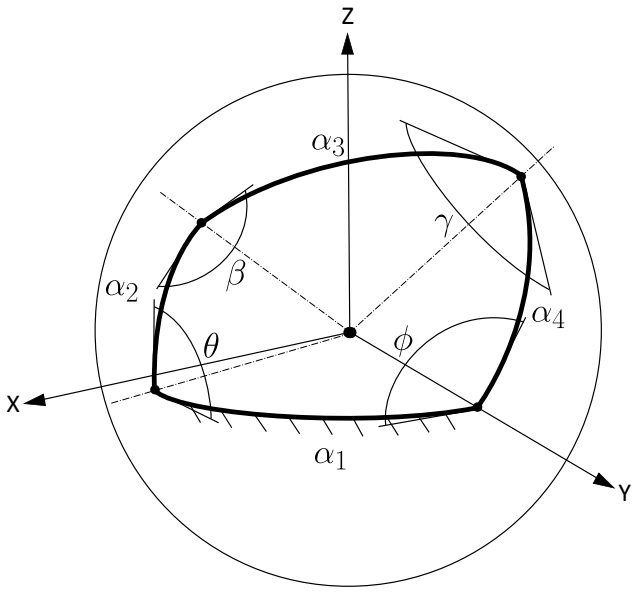

Figure 1.1: Skeleton diagram of a spherical 4R mechanism

Other areas of interest include 6-bar mechanisms and arrays. Numerous paper prototypes of these mechanisms have been created. To draw parallels to planar mechanisms, spherical versions of the Stephenson and Watt 6-bar chains were created, with their corresponding inversions (2 inversions for the Stephenson chain, and 1 inversion for the Watt Chain). Examples are shown in Figure 1.3. Mechanisms like these will be further developed and linked to the fundamentals mentioned above.

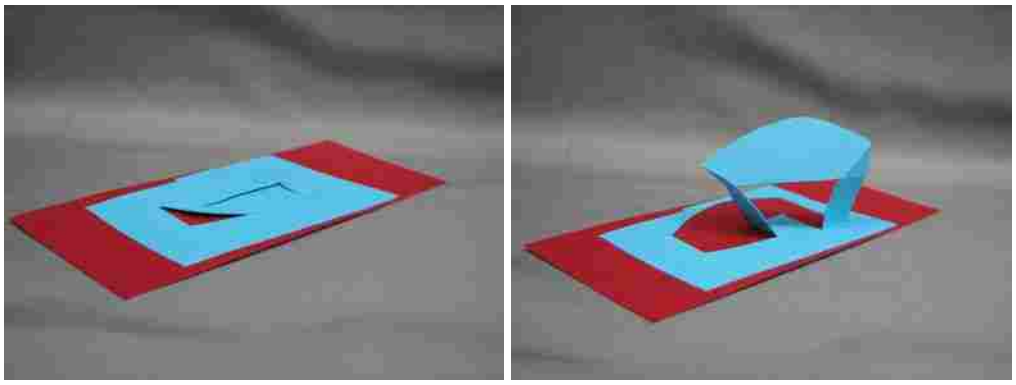

(a) Planar Position (b) Actuated Position

Figure 1.2: Spherical 4R LEM in its planar and actuated positions

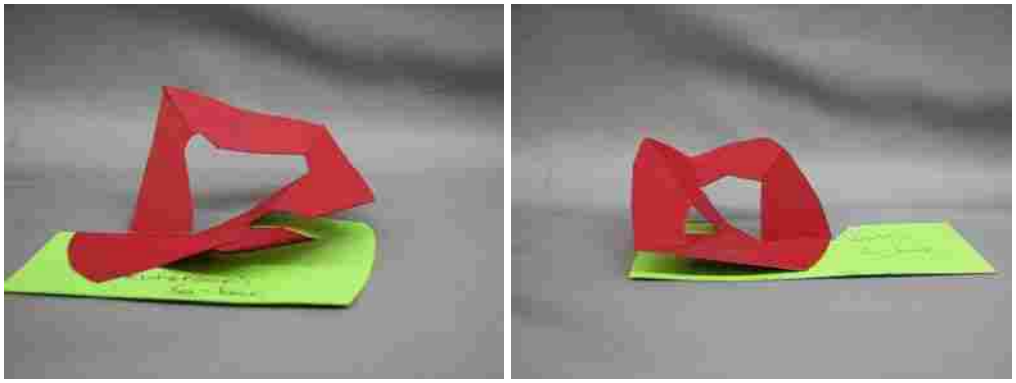

(a) Stephenson 6-bar chain (b) Watt 6-bar chain

Figure 1.3: Spherical LEM equivalents of a Stephenson 6-bar chain (left) and a Watt 6-bar chain (right)

1.1.2 LEM Joints

Finding suitable joints for use with compliant mechanisms can often be a challenge. The LET joint has been widely used in LEM applications [7]. Schematics of the LET joint are shown in Figure 1.4. This joint allows for high angular rotations about the y axis and possesses a simple topology. The challenge with working with the LET joint is its susceptibility to parasitic motion, especially when subjected to in subjected to in-plane compressive (see 1.4(a)) and tensile (see 1.4(b)) loads. Many applications would benefit from joints that are less susceptible to parasitic motion.

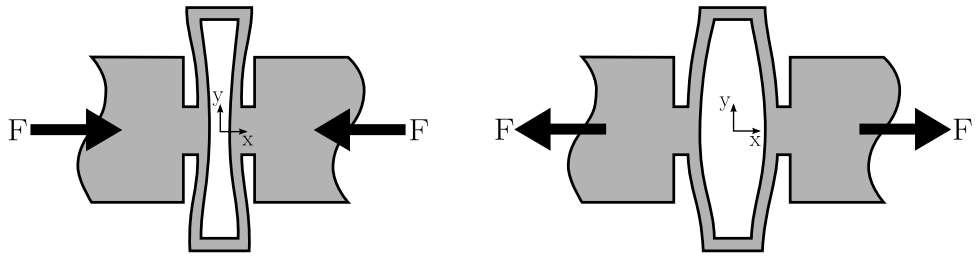

(a) LET joint loaded in compression (b) LET joint loaded in tension

Figure 1.4: Examples of parasitic motion in the LET joint

Winder et al. presented a way to simplify the creation of complex joints with LEMs and showed many prototypes of complex joints [10]. The research done by Jacobsen et al. and Winder et al. begins to expand the availability of LEM joints. A common concern with LEM joints is parasitic motion, especially when subjected to tensile or compressive loads. Joints designed to minimize parasitic motion will greatly benefit the field of LEMs. Currently, LEMs use living hinges, flexible beams, creases (in paper), and as previously mentioned, LET joints [2, 3, 7, 8, 10]. Other possibilities include creases in materials besides paper, compliant joints that allow complete revolution, and joints based on material properties and geometry, like the LET joint. A goal of this area of research is to provide additional joint options to designers based on design constraints.

CHAPTER 2. SPHERICAL LEMS[1]

The purpose of this chapter is to introduce spherical lamina emergent mechanisms and to describe the fundamentals that govern them. Lamina emergent mechanisms (LEMs) are compliant mechanical devices that are fabricated from planar materials with motion out of the fabrication plane [2]. As compliant mechanisms [11], LEMs achieve their motion by the deflection of flexible members. LEMs feature simple topology, but are capable of performing sophisticated tasks. The planar nature of LEMs allows them to be highly compact and suitable for fabrication by simple manufacturing processes. Most of the developments and applications of LEMs have been dedicated to planar mechanisms. In this chapter the capabilities and some of the possible applications of spherical LEMs are discussed.

For spherical mechanisms, any moving point is constrained to the surface of a sphere and the spherical surfaces are concentric [5]. Spherical mechanisms are the simplest mechanisms capable of spatial motion [4]. By their nature, spherical mechanisms are compact [5].

There is an opportunity to create mechanisms capable of spatial motion that are exceptionally compact by combining the spatial efficiency of spherical mechanisms and the planar nature of lamina emergent mechanisms. This combination is referenced to as "spherical lamina emergent mechanisms" and they show promise for applications where sophisticated motion is required in a small volume. This chapter identifies and classifies possible spherical LEMs. The classification includes all possible spherical 4R LEMs. By decomposition, more advanced mechanisms can be classified. The classification aids in predicting mechanism motion and in determining which mechanisms might be appropriate for particular applications. The classification builds on the classification scheme developed by Cervantes-Sánchez et al. [1] for rigid-link spherical mechanisms. This classification represents all possible spherical 4R linkages. It also lists all possible mechanisms, based on limits of link motion. It is based solely on link lengths and thus is readily applicable to

[1]The contents of this chapter have been accepted for publication in *Mechanism and Machine Theory* as "Spherical Lamina Emergent Mechanisms"

classification of spherical LEMs. Classification schemes group mechanisms based on there general characteristics. These characteristics can be used as a first step of synthesis purposes [12] and provide an overview of the design space for the mechanisms they concern. Many have been developed for planar [12–15], spherical [1, 5, 15, 16] and spatial mechanisms [17]. Tanik and Parlaktaş [18] describe a compliant RSSR mechanism capable of out-of-plane motion.

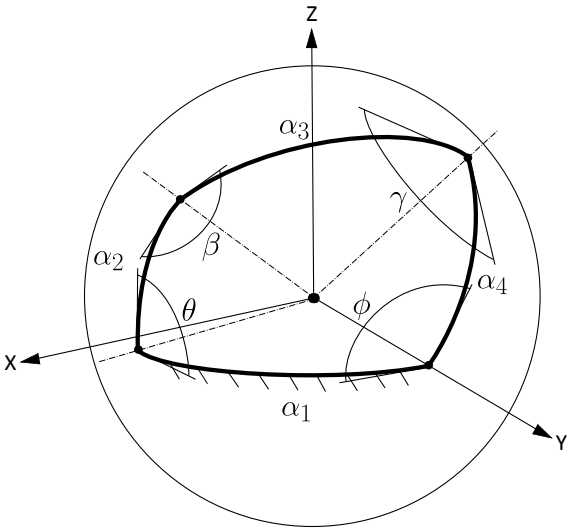

Figure 2.1: Skeleton diagram of a spherical 4R mechanism

2.1 Background

Cervantes-Sánchez et al. [1] defined a classification scheme for spherical 4R linkages. They conclude that there are 33 unique types of spherical 4R linkages. The classification is based on the range of motion of the links based on link lengths. Graphical representations of link mobility have also been developed by the same authors [19]. The mechanism types are distinguished by using designators of the form (a,b,c,d) where a,b,c, and d can take integer values from one to four and represent the limits of the angles θ, β, γ, and ϕ (see Figure 2.1 for angle definitions)[2]. The values of a,b,c, and d are determined using Equations (2.1) through (2.8) [1] and Table 2.1. Link lengths

are used to determine the compliance or violation of Equations (2.1) through (2.8). Then using Table 2.1, the designators (a,b,c,d) can be determined.

Equations in determining $a \in \{1,2,3,4\}$

$$\cos(\alpha_4 - \alpha_3) \geq \cos(\alpha_1 - \alpha_2) \tag{2.1}$$

$$\cos(\alpha_3 + \alpha_4) \leq \cos(\alpha_2 + \alpha_1) \tag{2.2}$$

Equations in determining $b \in \{1,2,3,4\}$

$$\cos(\alpha_1 - \alpha_4) \geq \cos(\alpha_3 - \alpha_2) \tag{2.3}$$

$$\cos(\alpha_4 + \alpha_1) \leq \cos(\alpha_2 + \alpha_3) \tag{2.4}$$

Equations in determining $c \in \{1,2,3,4\}$

$$\cos(\alpha_1 - \alpha_2) \geq \cos(\alpha_4 - \alpha_3) \tag{2.5}$$

$$\cos(\alpha_2 + \alpha_1) \leq \cos(\alpha_3 + \alpha_4) \tag{2.6}$$

Equations in determining $d \in \{1,2,3,4\}$

$$\cos(\alpha_3 - \alpha_2) \geq \cos(\alpha_1 - \alpha_4) \tag{2.7}$$

$$\cos(\alpha_2 + \alpha_3) \leq \cos(\alpha_4 + \alpha_1) \tag{2.8}$$

To further clarify Table 2.1, a designator value of "1" indicates the corresponding angle has no theoretical upper or lower limit. A "2" indicates the angle has an upper limit. A "3" indicates the angle has a lower limit, and a "4" indicates the angle has an upper and lower limit. The consequences of these limits are described in Table 2.1. The maximum and minimum values of each link angle are defined as

[2]Note: Cervantes-Sánchez et al. [1] use different link subscripts, with α_1 as the input link. In this chapter α_1 is the ground link.

Table 2.1: Spherical mechanism designation definitions [1]

Equation 2.1	Equation 2.2	Value	Definition
True	True	$a = 1$	θ has no upper or lower limit. The input link can fully rotate relative to the ground link.
True	False	$a = 2$	θ has an upper limit. The input link rocks between $\pm\theta_{max}$, passing through $\theta = 0^o$.
False	True	$a = 3$	θ has a lower limit. The input link rocks between $\pm\theta_{min}$, passing through $\theta = 180^o$.
False	False	$a = 4$	θ has an upper and lower limit. The input link rocks between θ_{min} and θ_{max} or $-\theta_{min}$ and $-\theta_{max}$.
Equation 2.3	Equation 2.4	Value	Definition
True	True	$b = 1$	β has no upper or lower limit. The coupler can fully rotate relative to the input link.
True	False	$b = 2$	β has an upper limit. The coupler link rocks between $\pm\beta_{max}$, passing through $\beta = 0^o$.
False	True	$b = 3$	β has a lower limit. The coupler link rocks between $\pm\beta_{min}$, passing through $\beta = 180^o$.
False	False	$b = 4$	β has an upper and lower limit. The coupler link rocks between θ_{min} and θ_{max} or $-\theta_{min}$ and $-\theta_{max}$.
Equation 2.5	Equation 2.6	Value	Definition
True	True	$c = 1$	γ has no upper or lower limit. The coupler can fully rotate relative to the output link.
True	False	$c = 2$	γ has an upper limit. The coupler link rocks between $\pm\gamma_{max}$, passing through $\gamma = 0^o$.
False	True	$c = 3$	γ has a lower limit. The coupler link rocks between $\pm\gamma_{min}$, passing through $\gamma = 180^o$.
False	False	$c = 4$	γ has an upper and lower limit. The coupler link rocks between γ_{min} and γ_{max} or $-\gamma_{min}$ and $-\gamma_{max}$.
Equation 2.7	Equation 2.8	Value	Definition
True	True	$d = 1$	ϕ has no upper or lower limit. The output link can fully rotate relative to the ground link.
True	False	$d = 2$	ϕ has an upper limit. The input link rocks between $\pm\phi_{max}$, passing through $\phi = 0^o$.
False	True	$d = 3$	ϕ has a lower limit. The input link rocks between $\pm\phi_{min}$, passing through $\phi = 180^o$.
False	False	$d = 4$	ϕ has an upper and lower limit. The input link rocks between ϕ_{min} and ϕ_{max} or $-\phi_{min}$ and $-\phi_{max}$.

$$\cos(\theta_{max}) = \frac{\cos(\alpha_3 + \alpha_4) - \cos(\alpha_2)\cos(\alpha_1)}{\sin(\alpha_2)\sin(\alpha_1)} \tag{2.9}$$

$$\cos(\theta_{min}) = \frac{\cos(\alpha_4 - \alpha_3) - \cos(\alpha_2)\cos(\alpha_1)}{\sin(\alpha_2)\sin(\alpha_1)} \tag{2.10}$$

$$\cos(\beta_{max}) = \frac{\cos(\alpha_4 + \alpha_1) - \cos(\alpha_2)\cos(\alpha_3)}{\sin(\alpha_2)\sin(\alpha_3)} \tag{2.11}$$

$$\cos(\beta_{min}) = \frac{\cos(\alpha_1 - \alpha_4) - \cos(\alpha_2)\cos(\alpha_3)}{\sin(\alpha_2)\sin(\alpha_3)} \tag{2.12}$$

$$\cos(\gamma_{max}) = \frac{\cos(\alpha_2 + \alpha_1) - \cos(\alpha_3)\cos(\alpha_4)}{\sin(\alpha_3)\sin(\alpha_4)} \tag{2.13}$$

$$\cos(\gamma_{min}) = \frac{\cos(\alpha_1 - \alpha_2) - \cos(\alpha_3)\cos(\alpha_4)}{\sin(\alpha_3)\sin(\alpha_4)} \tag{2.14}$$

$$\cos(\phi_{max}) = \frac{\cos(\alpha_2 + \alpha_3) - \cos(\alpha_4)\cos(\alpha_1)}{\sin(\alpha_4)\sin(\alpha_1)} \tag{2.15}$$

$$\cos(\phi_{min}) = \frac{\cos(\alpha_3 - \alpha_2) - \cos(\alpha_4)\cos(\alpha_1)}{\sin(\alpha_4)\sin(\alpha_1)} \tag{2.16}$$

2.2 Spherical LEMs

Spherical LEMs combine the compactness and simple topology of LEMs with the compact nature and three dimensional motions of spherical mechanisms. Spherical LEMs have similar features to those described by Lusk et al. [20] for microscale spherical mechanisms, in that the mechanism is manufactured in a planar position, the mechanism base (the sheet the mechanism was cut from) can cause interference, and there are geometric limitations on the orientation of the joint axes. Some examples of spherical LEMs are shown in [2, 8, 10]. Many of the prototypes created for this work use creases as joints, but other joints like the lamina emergent torsional (LET) [7] joint, and the joints discussed in Chapter 3 can also be used.

An example of a spherical 4R LEM is shown in Figure 2.2. This LEM was constructed of sheet steel. The joints have been plastically deformed, so that the mechanisms stays in a displaced position. The joints of this mechanism are LET joints which allow movement of the mechanism by torsion of long, thin segments [7]. This mechanism illustrates the planar nature of LEMs as well as the complex motion possible with spherical mechanisms.

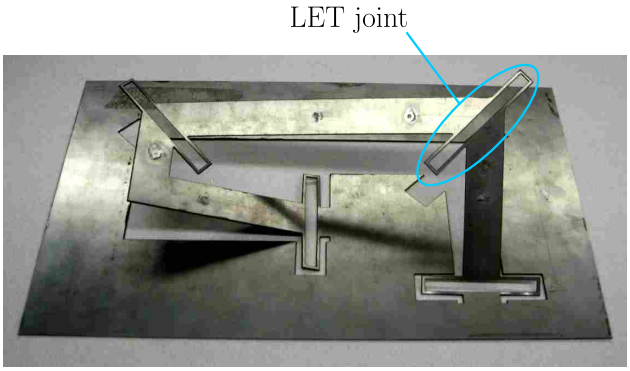

Figure 2.2: Spherical 4R LEM

For a spherical 4R mechanism to have a planar state (also referred to as the ability for a mechanism to fold [15]), one of the following equations must be true (see Figure 2.1 for link designations):

$$\alpha_1 + \alpha_4 = \alpha_2 + \alpha_3 \tag{2.17}$$

$$\alpha_1 + \alpha_2 = \alpha_3 + \alpha_4 \tag{2.18}$$

$$\alpha_1 + \alpha_3 = \alpha_2 + \alpha_4 \tag{2.19}$$

A mechanism whose link lengths satisfy Equation (2.17), (2.18) or (2.19) will be said to belong to spherical LEM Class Ia, Ib, or II, respectively. The spherical LEM classes organize the possible spherical 4R LEMs based on their layout in the planar position(s). As will be shown, many spherical mechanisms and arrays of spherical mechanisms can be reduced to a series of 4R linkages, so the criteria established here can be applied to mechanisms beyond the 4R linkage.

Figure 2.3 shows an example of a spherical 4R LEM that would belong to each class. The lines with long dashes represent revolute joints, or compliant joints with equivalent motion. The coordinate system is the same as that shown in Figure 2.1. It should be noted that if the output link and input link are switched, a Class Ia mechanism becomes a Class Ib mechanism, and vice versa. The input link must be specified to determine if the mechanism belongs to Class Ia or Ib. Class II is independent of the other two classes in that switching the input and output of a Class II mechanism becomes a different mechanism type, but remains Class II. This is due to fact that Class II mechanisms lay in a "crossed" configuration in one of their planar states (if their are multiple), meaning that the input and output links lay in opposite directions and will actuate in opposite directions, whereas for Class Ia and Class Ib, the input and output links lay in the same direction and actuate in the same direction.

2.2.1 Mechanism Possibilities for Each Class

To determine which mechanism types reported in [1] could be Class Ia spherical LEMs, Equation (2.17) was used in conjunction with Equations (2.1) through (2.8). An example of a Class Ia mechanism is shown in Figure 2.3(a). Combining Equations (2.17) and (2.1), we see that θ has no lower limit, thus $a \neq 3$ or 4. By combining Equations (2.17) and (2.4), it is found that β has no upper limit, thus $b \neq 2$ or 4. By similar methods, using Equations (2.5) and (2.8), γ has no lower limit, $c \neq 3$ or 4, ϕ has no lower limit, and $d \neq 2$ or 4.

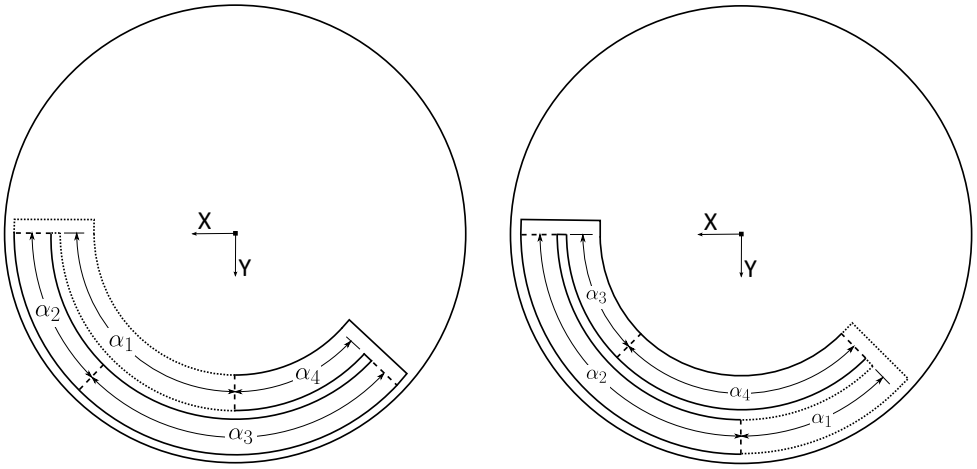

(a) Class Ia

(b) Class Ib

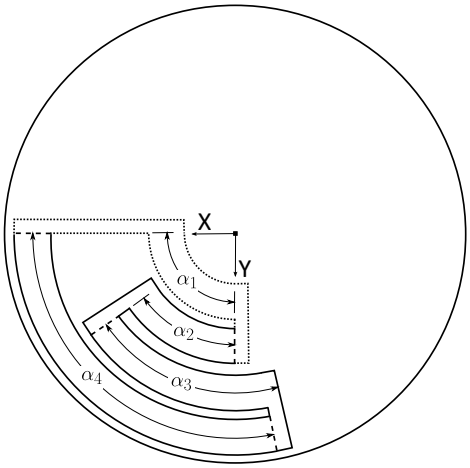

(c) Class II

Figure 2.3: Examples of mechanisms from the three classes

An example of a Class Ib mechanism is shown in Figure 2.3(b). Using the same method as was used for Class Ia, Equation (2.18) was combined with Equations (2.2), (2.3), (2.6) and (2.7). Thus, there is no upper limit on θ or γ and no upper limit on β or ϕ. Thus for a Class Ib, $a \neq 2$ or 4, $b \neq 3$ or 4, $c \neq 2$ or 4, and $d \neq 3$ or 4.

An example of a Class II mechanism is shown in Figure 2.3(c). Equation (2.19) was combined with Equations (2.1), (2.3), (2.5) and (2.7). Thus, there is no lower limit on θ, β, γ, or ϕ. For Class II, $a \neq 3$ or 4, $b \neq 3$ or 4, $c \neq 3$ or 4, and $d \neq 3$ or 4.

Using these inequalities, mechanisms were eliminated from the complete list of 33 spherical 4R LEMs created by [1]. A summary of each of the possible spherical 4R LEMs with their respective classes is shown in Table 2.2. The type numbers used in the table to not correspond to the mechanism numbers in [1].

Table 2.2: Spherical LEM classes and their corresponding 4R linkage types

Spherical LEM class	Type Numbers	Designation
Class Ia	1	(2, 3, 1, 1)
	2	(2, 1, 1, 3)
	3	(1, 3, 2, 1)
	4	(1, 1, 2, 3)
	5	(2, 1, 1, 1)
	6	(1, 1, 2, 1)
	7	(1, 3, 1, 1)
	8	(1, 1, 1, 3)
	9	(1, 1, 1, 1)
Class Ib	1	(3, 2, 1, 1)
	2	(3, 1, 1, 2)
	3	(1, 2, 3, 1)
	4	(1, 1, 3, 2)
	5	(1, 2, 1, 1)
	6	(1, 1, 1, 2)
	7	(3, 1, 1, 1)
	8	(1, 1, 3, 1)
	9	(1, 1, 1, 1)
Class II	1	(2, 2, 1, 1)
	2	(2, 1, 1, 2)
	3	(1, 2, 2, 1)
	4	(1, 1, 2, 2)
	5	(2, 1, 1, 1)
	6	(1, 1, 2, 1)
	7	(1, 2, 1, 1)
	8	(1, 1, 1, 2)
	9	(1, 1, 1, 1)

2.2.2 Class Summary

Many of the mechanisms shown in Table 2.2 indicate a fully rotating link (a, b, c, or $d = 1$). Note that this indication refers to ideal mechanism mobility and is based solely on link lengths, with no regard to joint capability or interference. Motion may be limited by the compliant joints or by link interference.

As shown in Table 2.2, there are 9 types of mechanism in each class, resulting in 27 mechanisms types. However, some mechanism types belong to multiple classes. This is caused by equalities in link lengths, resulting in multiple class conditions (Equations 2.17 through 2.19) be-

ing satisfied. Since the classification developed by [1]) is based strictly on limits of link motion, mechanism types that appear in multiple classes are only counted as one. mechanism types that appear in multiple classes will have the same limits on link motion, but different planar positions. This results in 21 types (of the 33 mechanisms from [1]) that can be spherical LEMs. Link angle equalities that cause mechanism types to appear in multiple classes are listed in Table 2.3. In these cases, the orientation of the links must be known to determine the mechanism class since the link lengths satisfy more than one planar position condition. Additionally, eliminating isomorphisms (see [11]) results in only 15 unique spherical 4R LEM types. These are shown in Table 2.4. It is interesting to note that when a mechanism's link lengths satisfy the conditions to be a Class Ia or a Class Ib mechanism ($\alpha_1 = \alpha_3$ and $\alpha_2 = \alpha_4$), the mechanism has two planar positions; one when $\theta = 0^\circ$ and one when $\theta = 180^o$ (see Figure 2.4). In this work, when the link lengths satisfy this condition the mechanism will be assumed to belong to Class Ia, meaning that the input link is chosen such that $\theta = 0^\circ$ in the mechanisms first planar position. Some Class II mechanisms are also capable of two planar positions; for example, when $\alpha_1 = 90^\circ, \alpha_2 = 45^\circ, \alpha_3 = 90^\circ$ and $\alpha_4 = 135^\circ$.

Table 2.3: Similarity of the mechanisms

Similar Mechanisms	Link Length Conditions
Class Ia Type 9 Class Ib Type 9	$\alpha_1 = \alpha_3$ and $\alpha_2 = \alpha_4$
Class Ia Type 5 Class II Type 5	$\alpha_1 = \alpha_2$ and $\alpha_3 = \alpha_4$
Class Ia Type 6 Class II Type 6	$\alpha_1 = \alpha_2$ and $\alpha_3 = \alpha_4$
Class Ib Type 5 Class II Type 7	$\alpha_1 = \alpha_4$ and $\alpha_2 = \alpha_3$
Class Ib Type 6 Class II Type 8	$\alpha_1 = \alpha_4$ and $\alpha_2 = \alpha_3$
Class II Type 9	$\alpha_1 = \alpha_2 = \alpha_3 = \alpha_4$

Each 15 mechanisms in Table 2.4 was prototyped using creased joints in planar materials. By changing which link was the input and accounting for all possible planar positions, these 15 prototypes represent all 27 mechanisms shown in Table 2.2. This is an effective way of quickly visualizing the motion, but has the limitation of possible interference between links. With LEMs, the range of joint motion and interference of links are often more limiting factors on motion than the mechanism type [10]. Knowing the mechanism type provides an understanding of possible linkage motion which will be advantageous in mechanism synthesis. From this starting point, the

Table 2.4: The 15 unique spherical 4R LEMs

Number	Isomorphic Mechanisms
1	Class Ia Type 1 Class Ib Type 4
2	Class Ia Type 2 Class Ib Type 2
3	Class Ia Type 3 Class Ib Type 3
4	Class Ia Type 4 Class Ib Type 1
5	Class Ia Type 5 Class Ib Type 6
6	Class Ia Type 6 Class Ib Type 5
7	Class Ia Type 7 Class Ib Type 8
8	Class Ia Type 8 Class Ib Type 7
9	Class Ia Type 9 Class Ib Type 9
10	Class II Type 1 Class II Type 4
11	Class II Type 2
12	Class II Type 3
13	Class II Type 5 Class II Type 8
14	Class II Type 6 Class II Type 7
15	Class II Type 9

link shapes and joints can be designed appropriately. An example of a prototype is shown in Figure 2.4. The link lengths of this mechanism are $\alpha_2 = 45^o$, $\alpha_3 = 90^o$, $\alpha_4 = 45^o$, and $\alpha_1 = 90^o$ which makes this mechanism a Class Ia, Type 9 (see Table 2.2). This mechanism is capable of two planar positions.

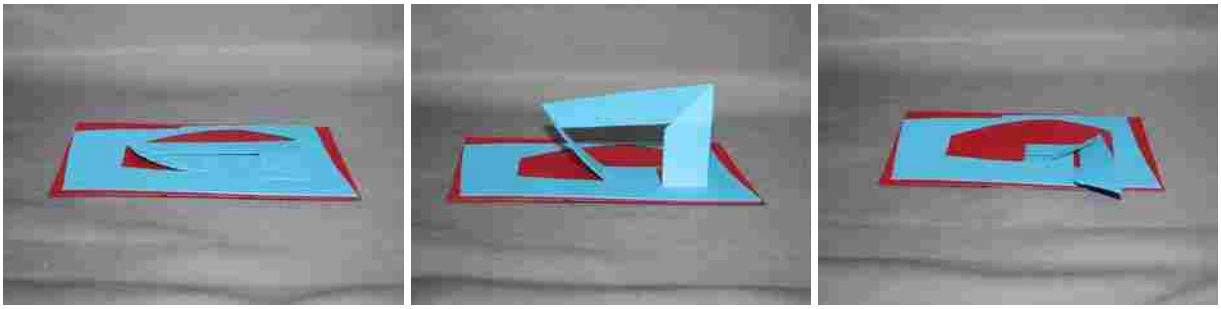

(a) In Planar Position (b) In an Actuated Position (c) In Second Planar Position

Figure 2.4: Spherical 4R LEM

2.2.3 Six-Bar Spherical LEMs

Spherical LEM equivalents of the Stephenson and Watt 6R chains are shown in Figures 2.5 and 2.6. The mechanism shown in these figures demonstrate the use arbitrary link shapes. However, even more so than with spherical 4R linkages, link collisions are common. The Stephenson chain is made of a spherical 4R and 5R chain, for which the analysis is more complicated than for the Watt chain, which can be modeled as two spherical 4R linkages (see [21] and [22] for more information on the analysis of the Stephenson chain). The Stephenson 6R can be simplified by a partial shrinkage of the ternary link (not the ground link) [23]. This results in two serially connected 4R linkages that share the same sphere center. Examples of these types of mechanisms are shown in Section 2.2.4 of this work.

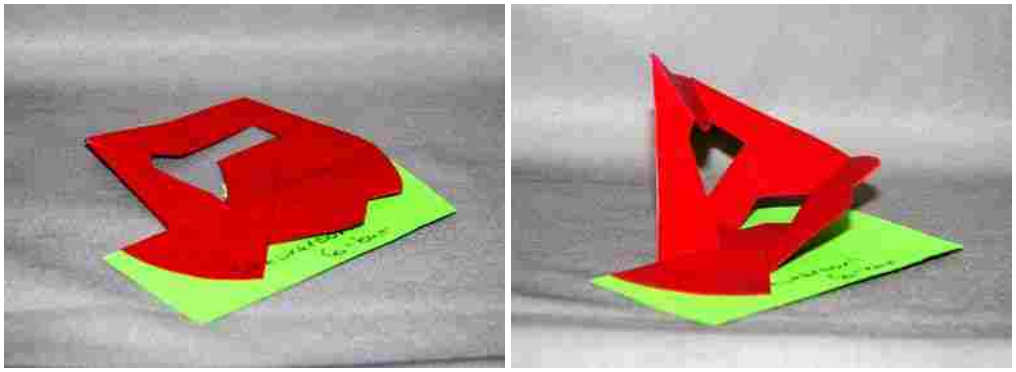

(a) In Planar Position (b) In Actuated Position

Figure 2.5: Spherical 6R LEMs - Stephenson Chain

2.2.4 Arrays of Spherical LEMs

A LEM array is a patterned arrangement of LEMs [3]. This section derives patterned arrangements of spherical 4R linkages. Figure 2.7 is an array of two 4R LEMs. The serially connected spherical 4R linkage discussed by Makhsudyan et al. [9] is the basis of many of the following arrays. The output link of one 4R linkage is the input link to the other linkage. Notice the two 4R linkages do not share the same sphere center. However, the sphere centers do share a common axis. Continuing the same pattern of serially connected 4R chains, the array shown in

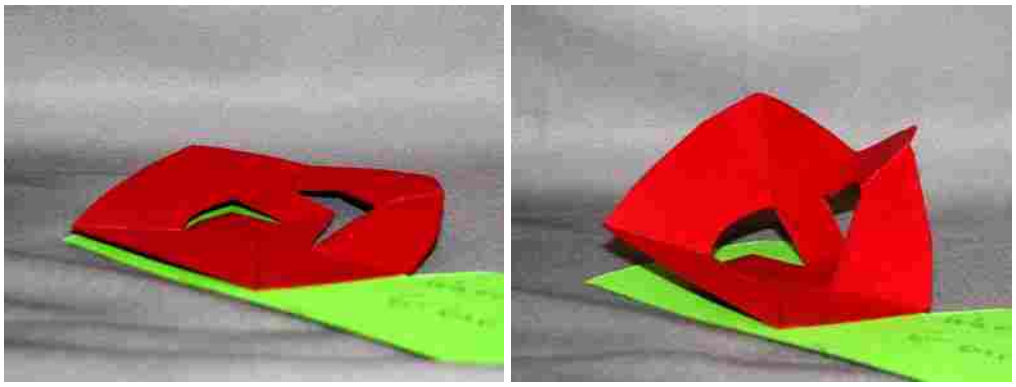

(a) In Planar Position (b) In Actuated Position

Figure 2.6: Spherical 6R LEMs - Watt Chain

Figure 2.8 contains four spherical 4R linkages, and four separate sphere centers. These arrays are built from identical 4R linkages. The resulting nine link mechanism is still a 1 DOF linkage. Actuating one 4R linkage actuates the entire array. This pattern could be extended to as many spherical mechanisms as is necessary. Notice that in Figure 2.8, the links of the spherical mechanism become disguised to demonstrate the ability to move desired shapes. The link lengths of each of the 4R linkages in the arrays shown in Figures 2.7 and 2.8 are $\alpha_1 = \alpha_3 = 90^o$, $\alpha_2 = \alpha_4 = 45^o$. With these link lengths, the 4R linkages are Class Ia, Type 9 mechanisms. Because Class Ia, Type 9 4R linkages are capable of two planar positions, the arrays are also capable of 2 planar positions.

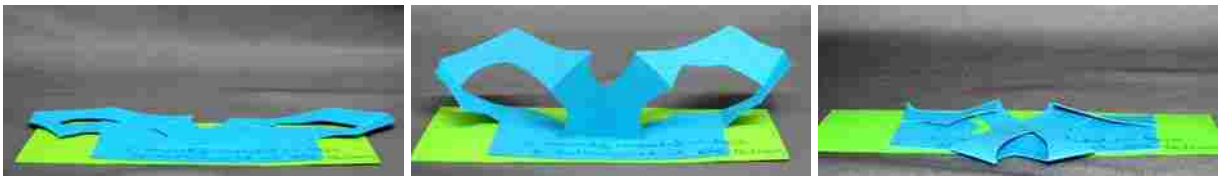

(a) In Planar Position (b) In Actuated Position (c) In Second Planar Position

Figure 2.7: Two serially connected 4R LEMs

The array of spherical mechanisms shown in Figure 2.9 is similar to that shown in Figure 2.8 in that it is four serially connected 4R linkages, but the link lengths are different in this case. Taking the longer side of the box as the input link, the link lengths of each mechanism are $\alpha_2 = 90^o$,

$\alpha_3 = 45^o$, $\alpha_4 = 135^o$, and $\alpha_1 = 90^o$. These linkages are Class Ib, Type 7 mechanisms (see Table 2.2). For this type of mechanism, the input link is limited by $\pm\theta_{min}$, as defined by Equation (2.10). For this array, $\theta_{min} = 90^o$. In the planar state, $\theta = 180^o$ and the input link can move to $\pm 90^o$. In its fully actuated position, $\theta = 90^o$ for each 4R linkage in the array. Because the output links of each 4R linkage are the input links of another, those links are also limited to $\pm\theta_{min}$. Notice that in contrast to the array in Figure 2.8, the "walls" (input and output links) of this array all reach 90^o at the same time and are limited in motion at that point.

(a) In Planar Position (b) In Actuated Position (c) In Second Planar Position

Figure 2.8: Four serially connected 4R LEMs

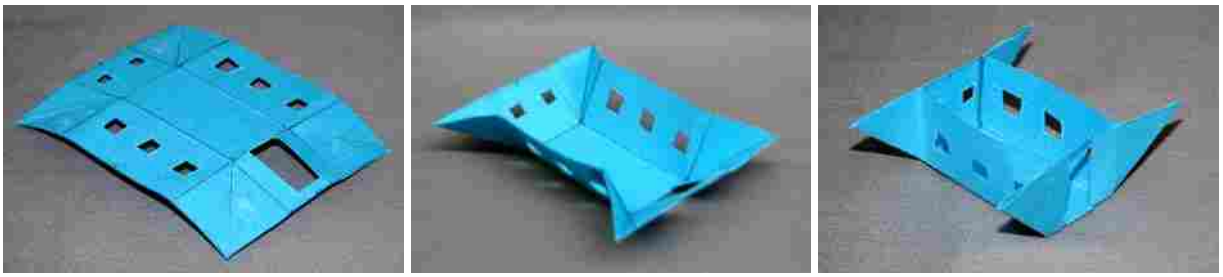

(a) In Planar Position (b) Partially Actuated Position (c) In Actuated Position

Figure 2.9: Four serially connected 4R LEMs

The array in Figure 2.10 also features four serially connected spherical 4R linkages. Let the input links be the faces that fold towards the middle in the planar position. The link lengths for each spherical 4R linkage are $\alpha_2 = 90^o$, $\alpha_3 = 45^o$, $\alpha_4 = 45^o$, and $\alpha_1 = 90^o$. With these link lengths, the 4R linkages are Class Ia, Type 5 mechanisms. The input link is limited by $\pm\theta_{max}$ as defined by

(a) In Planar Position (b) Partially Actuated Position (c) In Actuated Position

Figure 2.10: Four serially connected 4R LEMs

Equation (2.9). For the 4R linkages in this array, $\theta_{min} = 90^o$, and $\theta = 0^o$ in the planar position. In the fully actuated position $\theta = 90^o$ for each 4R linkage. As with the previous example, the input and output links all reach 90^o at the same time and are limited in motion at that point. Although all three of the arrays discussed thus far have many similar characteristics, it has been shown that by decomposing the array into its spherical 4R linkages, the classification scheme developed by [1] and applied to spherical LEMs in this work can be used to predict the motion of the array as well as the limits of movement.

A different form of a spherical LEM array is a multi-layer LEM, or MLEM [6]. An example is shown in Figure 2.11. This mechanism is two serially connected 4R mechanisms on bottom, and two on top, sharing the same sphere center. It is interesting to note that even small inputs to the bottom mechanism quickly cause the motion of the top mechanism to reach its limit. The link lengths of the two mechanisms are identical, although the top mechanism is rotated 90^o relative to the bottom mechanism. The link lengths are the same for all 4R linkages in this array; $\alpha_1 = \alpha_3 = 90^o$ and $\alpha_2 = \alpha_4 = 45^o$, making each of the 4R linkages a Class Ia, Type 9 mechanism, capable of two planar positions. Connected as they are, the array is not capable of two planar positions due to interference between the top and bottom arrays.

Another form of a spherical LEM array is shown in Figure 2.12. This mechanism is four serially connected 4R linkages, all sharing the same sphere center. This array could also be modeled as two serially connected Stephenson 6R chains with partial shrinkage of their ternary links as previously discussed. The linkages ”spiral” around the sphere center. This layout is similar to that used by Lusk et al. [24] on their Micro Helico-Kinematic Platform that involves an array of three

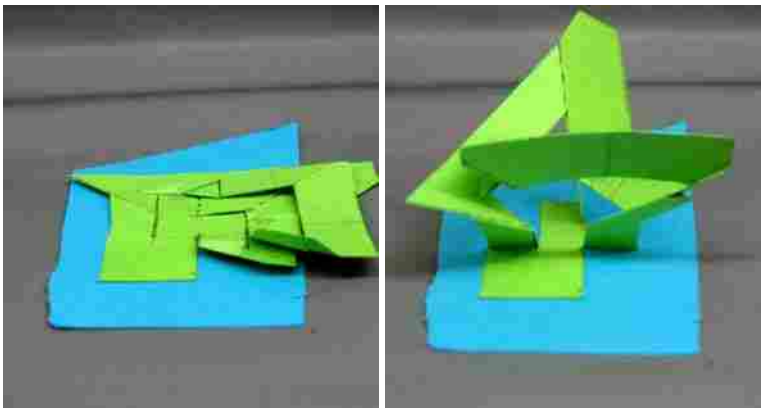

(a) In Planar Position (b) In Actuated Position

Figure 2.11: Multi-layer LEM

spherical crank sliders that share the same sphere center. Although the mechanism shown in Figure 2.12 appears complex, it can be decomposed into simple 4R linkages. For each 4R linkage in this prototype, $\alpha_1 = \alpha_3 = 90^o$ and $\alpha_2 = \alpha_4 = 45^o$. Each 4R linkage is a Class Ia, Type 9 mechanism, capable of two planar positions.

(a) In Planar Position (b) In an Actuated Position (c) In Second Planar Position

Figure 2.12: Four serially connected spherical 4R LEMs sharing the same sphere center

2.3 Conclusions

A classification for spherical 4R LEMs was developed and the different types of possible spherical 4R LEMs were reported. Each of these mechanism types has unique motion characteristics which can be used as a starting point for mechanism synthesis. Examples of spherical 6R LEMs were demonstrated. Arrays of spherical 4R LEMs were prototyped and based on the types

of spherical 4R linkages in the array, the motion of the array can be predicted. Other types of arrays were also demonstrated. These included MLEMs and multiple spherical 4R linkages that share the same sphere center. It has been shown that this classification can be extended to spherical mechanisms beyond the 4R by decomposing the linkage into its respective 4R chains. Based on the classification of the 4R chains, the motion of the entire linkage can be predicted.

The extreme compactness of spherical LEMs makes them candidates for application with require complex motion using a small volume (e.g. space applications and deployable systems) and may be used as fundamental components in future surface morphing applications.

CHAPTER 3. LEM JOINTS[1]

Lamina emergent mechanisms (LEMs) are compliant mechanisms that can be fabricated from planar sheets [2]. Upon actuation, LEMs "emerge" out of the fabrication plane. A preliminary study of LEM joints was performed by Winder et al. which discusses a method of using serial chain approximations to create LEM joints with the desired characteristics [10]. Multiple applications of LEMs have been proposed [3] ranging from disposable mechanisms to deployable mechanisms. Other emerging areas of application for the proposed joints, and for LEMs as a whole, include adaptive morphing structures and engineering applications of origami principles. An example of a LEM is shown in Figure 3.1.

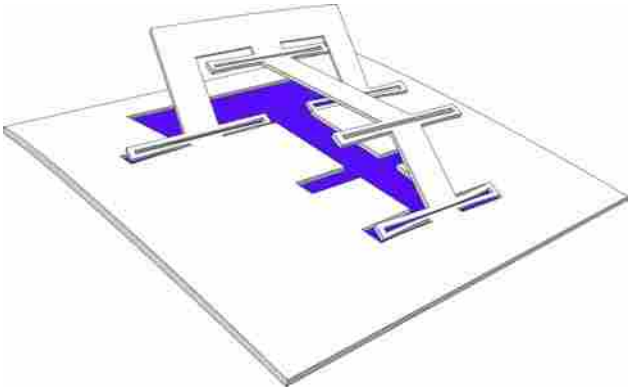

Figure 3.1: LEM 4R linkage

LEMs offer the advantages of a topology compatible with planar layers, inherent compactness, and compatibility with simple manufacturing processes in addition to the advantages currently possessed by compliant mechanisms. Also, many LEMs posses a monolithic structure. The advantages of a monolithic structure, as well as advantages of compliant mechanisms are discussed

[1]The contents of this chapter have been submitted for publication in *Mechanism and Machine Theory* as "Introduction of Planar Compliant Joints Designed for Compression and Tension Loading Conditions in Lamina Emergent Mechanisms"

in [25]. Thorough documentation on the advantages and disadvantages of compliant mechanisms can be found in [11].

Lamina emergent torsional (LET) joints [7] have been finding use in LEMs; however, they do not lend themselves well to applications where the joints experience significant tension or compression loads because they allow considerable parasitic motion under those conditions. An example of designing for parasitic motion in LET joints is shown in [26], where the authors use a minimum potential energy optimization to determine the position of a fully compliant mechanism, taking into account the parasitic motion of the joint.

This chapter introduces three joints that are compatible with lamina emergent mechanisms (LEMs). LET joints are used as a benchmark comparison for the joints. For each joint, a LET joint was modeled to have the same bending stiffness and maximum axial (tensile and/or compressive) stiffness. The compressive and/or tensile stiffnesses of the joints were then compared. The new joints exhibit increased off-axis stiffness (reduced parasitic motion) compared to the LET joint when subjected to compressive and/or tensile loads.

3.1 Background

Designing LEMs can be challenging because all mechanism components are confined to the plane of fabrication. Joint design can be particularly challenging. Jacobson et al. [7] developed the lamina emergent torsional (LET) joint; a LEM compatible joint that allows for large rotations in situations where off-axis stiffness is not critical. Off-axis stiffness is defined as the stiffness in any direction other than the desired motion of the joint [27], and greater off-axis stiffness results in reduced parasitic motion. Ferrell et al. [28] describe LEM joints with specific application to metals. Other work in compliant joints, while not restricted to LEMs, addresses many of the challenges of compliant joints. For example, Trease et al. discuss large-displacement compliant joints [27]. Yao et al. kinematically describe the folding of cartons where creases act as joints [29]. Zhao et al. discuss a monolithic flexural pivot [30]. Pei et al. discuss the design of cartwheel flexural hinges [31]. Dai and Jones discuss the modeling of metamorphic structures that begin as flat sheets and through folding become a structure [32].

3.1.1 Isolation and Inversion

Compression of compliant joints is often a concern and many compliant joints are not able to adequately support compressive loads. Guérinot et al. [33] describe two methods, isolation and inversion, for increasing the amount of compressive load a compliant joint can carry. Isolation is accomplished by diverting the compressive load from the flexible segment(s) to a rigid element(s) of the joint. An example is a passive rest that comes into contact when the joint is put in compression. Isolation is often a challenge with LEMs. Because the joint is restricted to a plane, areas that come into contact are small, making the passive rests unstable. More rests can be added, but they will be coplanar for a single layer LEM. Inversion is more applicable to LEMs. Inversion involves reconfiguring the joint so that the members prone to buckling are put in tension when the joint is compressed.

3.1.2 The Lamina Emergent Torsional (LET) Joint

The LET joint, shown in Figure 3.2(a), will be used as a benchmark for comparison of the new joints. The LET joint described here is assumed to be symmetric about the x and y axes. The subscripts of the k labels in Figure 3.2(a) indicate the primary deflection mode of the labeled member when the joint is deflected about the y axis: b represents bending and t represents torsion. A linear spring model is shown in 3.2(b). This model will be used to determine a closed-form model of the stiffness in bending about the y axis. The dimension labels used for the stiffness derivation and throughout this work for the LET joint are shown in Figure 3.3.

As developed in [7], the bending stiffness of the LET joint can be derived as

$$k_{eq,bend} = \frac{2k_{tl}k_{bl}}{k_{tl}+2k_{bl}} \tag{3.1}$$

where

$$k_{bl} = \frac{Ew_{bl}t^3}{12l_{bl}} \tag{3.2}$$

and

$$k_{tl} = w_{tl}t^3\frac{G}{l_{tl}}\left[\frac{1}{3} - 0.21\frac{t}{w_{tl}}\left(1-\frac{t^4}{12w_{tl}}\right)\right] \tag{3.3}$$

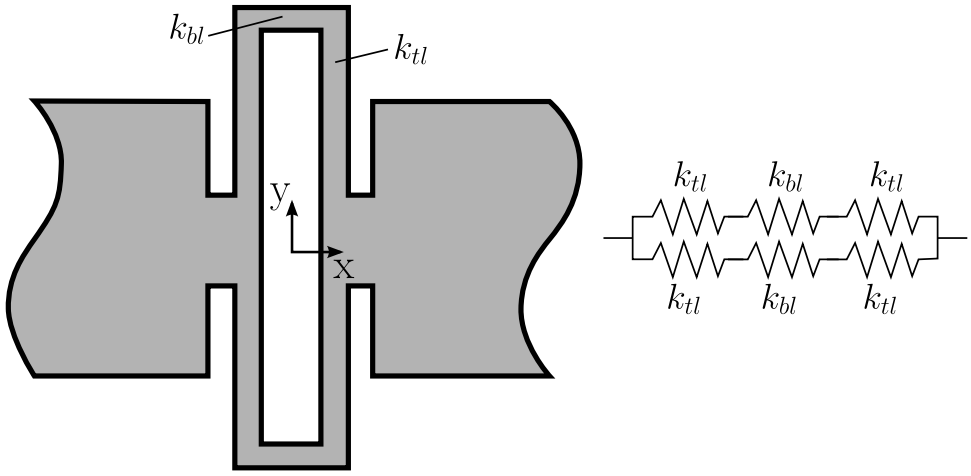

(a) The LET joint (b) Spring model of the LET joint

Figure 3.2: Lamina Emergent Torsional (LET) joint and its associated spring model

In Equations (3.1) through (3.3), t represents the thickness of the material, E represents the modulus of elasticity, and G represents the modulus of rigidity. Equation 3.3 is used to describe a rectangular beam in torsion [34]. For all the analyses in this work, the material was assumed to be polypropylene; with $E = 1.4\ GPa, \nu = 0.42$, and $G = 0.493\ GPa$.

Assuming the bending segments of the joint are considered to be completely rigid in tension and compression (along the x axis), i.e. $k_{bl} = \infty$, and assuming small deflections, the compressive ($k_{eq,comp}$) and tensile (k_{eq_tens}) stiffnesses of the joint can be modeled as

$$k_{eq,comp} = k_{eq,tens} = \frac{Etw_{tl}^3}{l_{tl}^3} \tag{3.4}$$

This model is valid for small deflections and assumes the bending segments of the joint can be modeled as rigid. This model is particularly useful when combined with an optimization algorithm, as discussed later. When this simplified model is inadequate, nonlinear finite element analysis will be used.

The LET joint is capable of large angular deflections and is geometrically simple, making it easy to implement in LEMs. The disadvantages of the LET joint include low off-axis stiffness

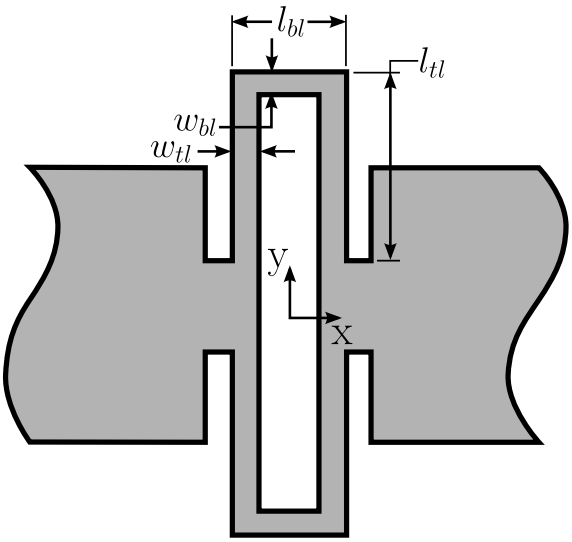

Figure 3.3: Dimension labels for the LET joint

and a potential for parasitic motion under tension and compression loading. Note that it is assumed that the tension and compression loading is completely in the *xy* plane. This is illustrated in Figure 3.4. In this chapter the LET joint is used as a benchmark for the other joints.

3.1.3 Method

The following steps will be used in the development and evaluation of the new joints:

1. Develop a closed-form model of joint bending stiffness
2. Use the closed-form model to optimize joint geometry for minimum bending stiffness, assuming material properties and material thickness are constant
3. Create an FEA model of the joint being studied using the optimized dimensions to obtain a more accurate bending stiffness value and to determine the compressive and/or tensile stiffness(es) value(s)
4. Optimize the benchmark LET joint geometry to match the bending stiffness to that obtained in the previous step and maximize compressive and/or tensile stiffness(es)

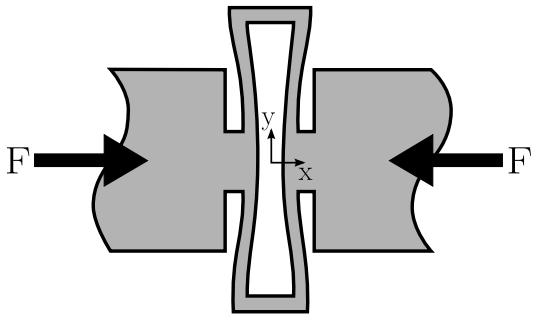

(a) LET joint loaded in compression

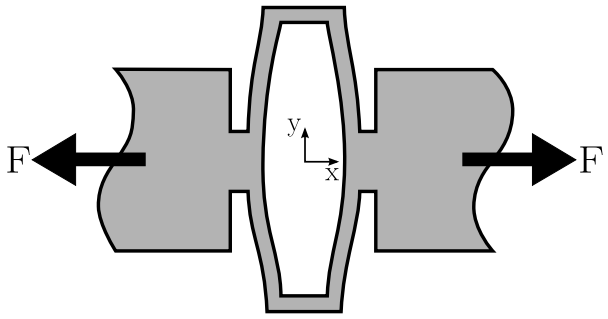

(b) LET joint loaded in tension

Figure 3.4: Examples of parasitic motion in the LET joint

5. Create an FEA model of the LET joint using optimized dimensions to obtain a more accurate bending and compressive and/or tensile stiffness(es) value(s)

6. Compare stiffness results from FEA models

These steps were used for each of the three joints introduced in this chapter. The LET joint is used as a benchmark of comparison to demonstrate the new joints' advantages and disadvantages.

3.2 The Inverted LET (I-LET) Joint

The Inverted LET (I-LET) joint was designed using the principle of inversion [33] and is capable of bearing compressive loads with reduced parasitic motion compared with the LET joint. Its name comes from the fact that the long bending members (labeled k_{b2} in Figure 3.5(a)) are put

in tension when the joint is loaded in compression (along the $-x$ axis). This joint, with its corresponding spring model, is shown in Figure 3.5. Most of the movement of this joint comes from the bending of long, flexible segments, although some torsion is present in the torsion members aligned with the y axis. The bending members are oriented so that when the joint is loaded in compression, they are loaded in tension.

3.2.1 Closed-Form Model

A closed-form model of the joint's bending stiffness was developed. Referring to the model shown in Figure 3.5(b) and the dimensions indicated in Figure 3.6, the bending stiffness ($k_{eq,bend}$) of the joint was derived assuming small deflections and pure moment loading:

$$k_{eq,bend} = \frac{2k_{b1}k_{b2}k_{b3}k_{b4}k_{t1}k_{t2}k_{t3}}{k_{sum}k_{b4} + 2k_{b1}k_{b2}k_{b3}k_{t1}k_{t2}k_{t3}} \tag{3.5}$$

where

$$\begin{aligned} k_{sum} = {} & k_{b1}k_{b2}k_{b3}k_{t2}k_{t3} + k_{b1}k_{b2}k_{b3}k_{t2}k_{t3} + k_{b1}k_{b2}k_{b3}k_{1t}k_{t3} \\ & + k_{b1}k_{b3}k_{t1}k_{t2}k_{t3} + k_{b1}k_{b2}k_{b3}k_{t1}k_{t2} + k_{b1}k_{b2}k_{t1}k_{t2}k_{t3} \end{aligned} \tag{3.6}$$

and

$$k_{b1} = \frac{Ew_{b1}t^3}{12l_{b1}} \tag{3.7}$$

$$k_{b2} = \frac{Ew_{b2}t^3}{12l_{b2}} \tag{3.8}$$

$$k_{b3} = \frac{Ew_{b3}t^3}{12l_{b3}} \tag{3.9}$$

$$k_{b4} = \frac{Ew_{b4}t^3}{12l_{b4}} \tag{3.10}$$

$$k_{t1} = w_{t1}t^3\frac{G}{l_{t1}}\left[\frac{1}{3} - 0.21\frac{t}{w_{t1}}\left(1 - \frac{t^4}{12w_{t1}^4}\right)\right] \tag{3.11}$$

$$k_{t2} = w_{t2}t^3\frac{G}{l_{t2}}\left[\frac{1}{3} - 0.21\frac{t}{w_{t2}}\left(1 - \frac{t^4}{12w_{t2}^4}\right)\right] \tag{3.12}$$

$$k_{t3} = w_{t3}t^3\frac{G}{l_{t3}}\left[\frac{1}{3} - 0.21\frac{t}{w_{t3}}\left(1 - \frac{t^4}{12w_{t3}^4}\right)\right] \tag{3.13}$$

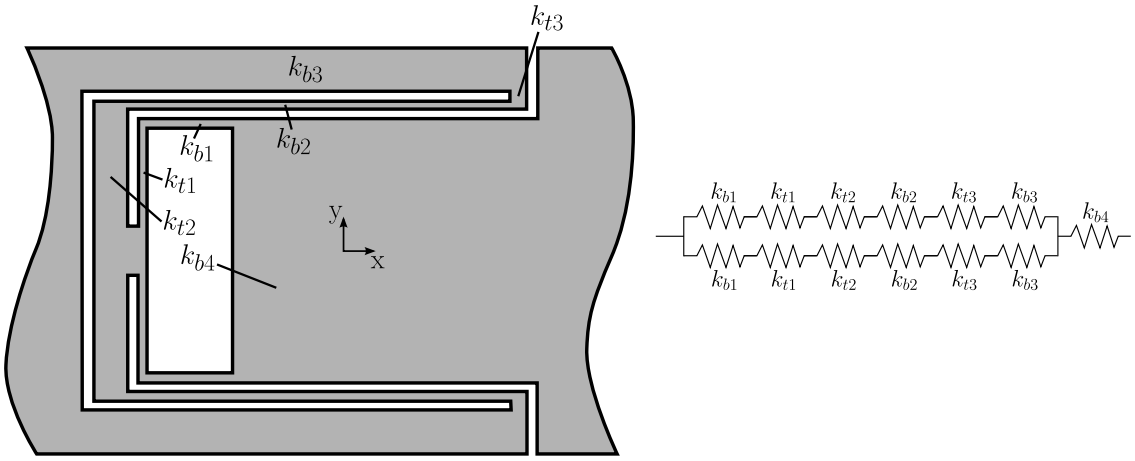

(a) The I-LET joint (b) Linear spring model

Figure 3.5: Inverted LET (I-LET) joint and its associated linear spring model

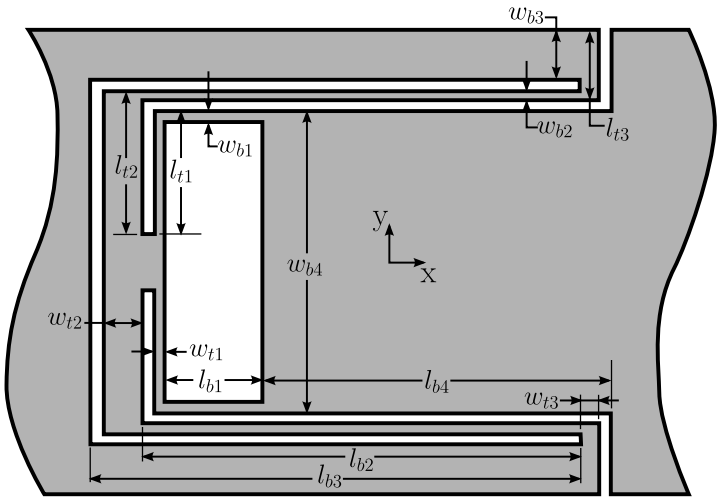

Figure 3.6: Dimension labels for the I-LET joint

The closed-form stiffness model shown in Equation (3.5) was used to optimize the I-LET joint geometry, where $k_{eq,bend}$ was minimized. The optimization constraints were based on manufacturing constraints and geometry that was constrained to a 50 mm long by 46 mm wide area. 46 mm was chosen as the width so that when the tension straps (which are discussed later) are added,

the joint is constrained to a 50 mm by 50 mm area. A GRG algorithm was used for the optimization since the closed-form equations are well behaved and the algorithm quickly converged. The optimized dimensions are listed in Table 3.1. This geometry was used to model the joint using a finite element analysis (FEA) program capable of nonlinear analysis (ANSYS® [35]). Since the joint is symmetric, only half of it was modeled to save computation time. The joint was fixed at one end and the free end was constrained to go through a specified rotation of 30° (0.524 rad) for bending and through an axial deflection of 0.2 mm in the $-x$ direction for in-plane compression. The deflected FEA bending model is shown in Figure 3.7.

Table 3.1: Dimensions of the I-LET joint optimized for minimum bending stiffness

Dimension	Value (mm)	Dimension	Value (mm)
l_{b1}	8	l_{t1}	12
w_{b1}	1	w_{t1}	1
l_{b2}	43	l_{t2}	14
w_{b2}	1	w_{t2}	4
l_{b3}	47	l_{t3}	7
w_{b3}	5	w_{t3}	2
l_{b4}	36	t	1
w_{b4}	30		

3.2.2 FEA Model

Using the dimensions obtained from the optimization, an FEA model of the I-LET joint was created. To compare the compressive stiffness of the I-LET joint to the LET joint benchmark, a LET joint was optimized for maximum stiffness in compression, while maintaining the same bending stiffness as the optimized I-LET joint. The total width of the optimized LET joint was 57.71 mm. The other optimized dimensions are listed in Table 3.2. See Figure 3.3 for associated dimension labels. These dimensions were used in an FEA model of the LET joint using the same boundary conditions as those for the I-LET joint. All the FEA models for this work were created using shell (ANSYS SHELL93) elements. The I-LET model contained 8943 elements, and the benchmark LET joint model contained 2534 elements.

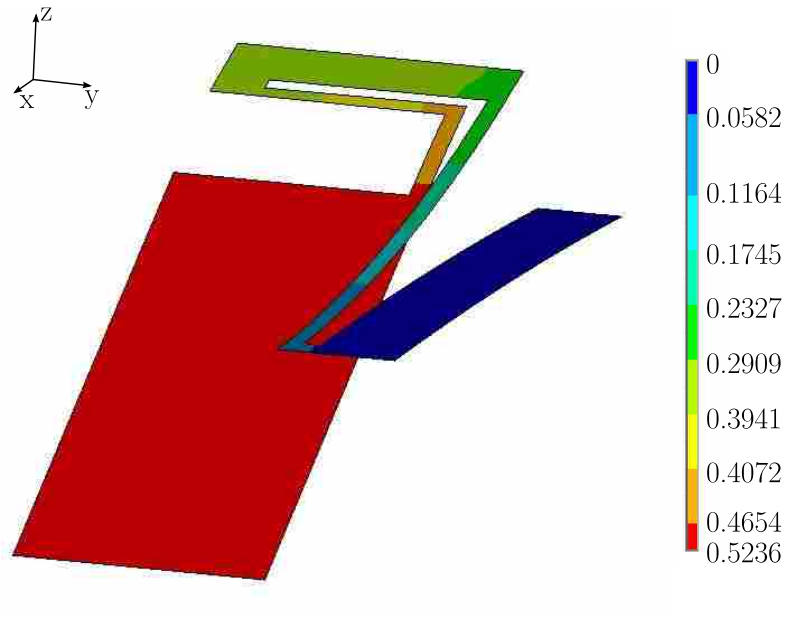

Figure 3.7: FEA model of the I-LET joint showing the deflected position in bending, indicating rotation about the *y* axis

Using the FEA models, the reaction moments (in the case of bending) and forces (in the case of compression) were used to find the stiffnesses of the joints. Table 3.3 summarizes the results. The ideal value for the ratio of the $k_{eq,bend}$ values is 1. With a similar bending stiffness to that of the LET joint, the I-LET is 13 times more stiff in compression. It should be noted that the closed-form model of the LET joint's compressive stiffness predicted a value 14.5% greater than that of the FEA model. This is caused by the fixed-guided boundary conditions used in the closed-form model, and result in an over-prediction of the LET joints compressive (and tensile)

Table 3.2: Dimensions of a LET joint optimized for a bending stiffness equivalent to the I-LET joint and maximum compressive stiffness

Dimension	Value (mm)
l_{bl}	4
w_{bl}	1
l_{tl}	25.858
w_{tl}	1
t	1

stiffness. For all the LET joint geometries in this work, the closed-form model over-predicted the tensile and compressive stiffness.

Table 3.3: Comparison of joint stiffnesses: I-LET and LET joints

	I-LET Joint	LET Joint	Ratio
$k_{eq,bend}(N \cdot mm/rad)$	2.567	2.593	0.99
$k_{eq,comp}(N/m)$	921.2	70.73	13.02

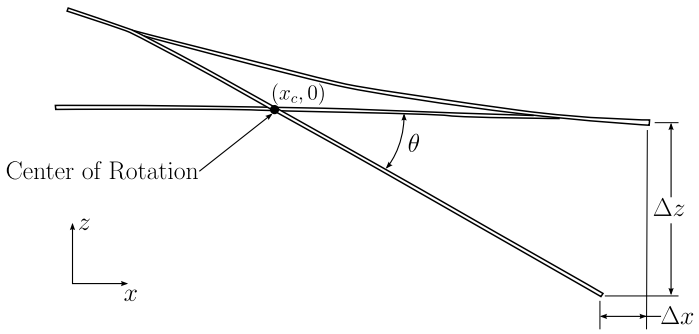

Figure 3.8: Side view of deflected I-LET

The I-LET joint can effectively bear compressive loads. Its disadvantages include the large area the joint takes up compared to the LET joint. Also, the joint is not suitable for high shear loading, where one end of the joint is loaded in the positive y direction, and the other end in the negative y direction. Another concern with the I-LET joint is the movement of the center of rotation throughout the motion of the joint. A side view of the deflected joint is shown in Figure 3.8. The position of the center of rotation is designated as $(x_c,\ z_c)$. Throughout the motion of the joint,

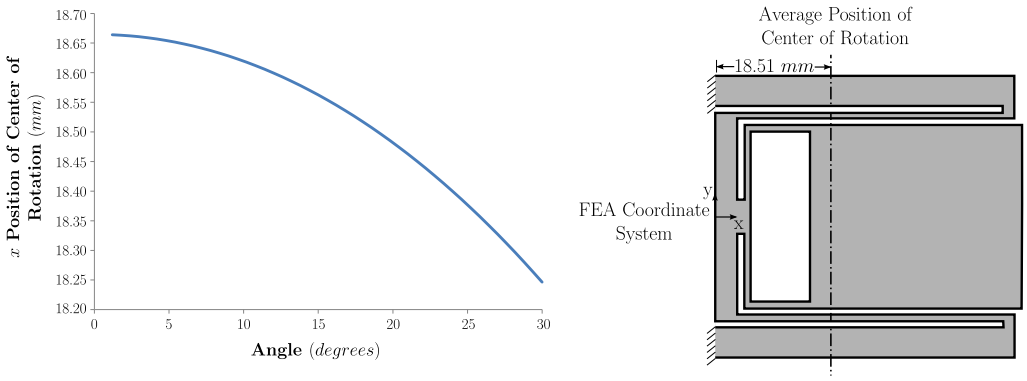

(a) x_c plotted against angle of rotation

(b) Average position of the center of rotation of the I-LET joint for a 30° rotation

Figure 3.9: Determining the center of rotation of the I-LET joint

$z_c = 0$. x_c can be found using the following equation:

$$x_c = l_j + \Delta x + \frac{\Delta z}{\tan\theta} \tag{3.14}$$

where l_j represents the total length of the joint. The x position of the center of rotation is plotted against angle of rotation in Figure 3.9(a). The center of rotation moves 0.418 mm in the $-x$ direction through the 30° motion of the joint, or 0.84% of the total length of the joint. The average position of the center of rotation, $x_{c,average}$ is 18.51 mm from the fixed end of the joint, if the FEA models coordinate system is used. The average position of the center of rotation through a deflection of 30° is shown in Figure 3.9(b).

3.2.3 Alternative Configuration

If additional compressive stiffness is desired, at the expense of bending flexibility, the I-LET can be configured as shown in Figure 3.10. The equations developed previously for the I-LET joint still apply, but k_{b1} and k_{t1} are no longer part of the equations. Using the same dimensions as those used previously, the bending stiffness of this configuration is 3.733 $N \cdot mm/rad$, 1.45 times larger than the bending stiffness of the baseline configuration. The compression stiffness is 7531 N/m, or 8.17 times greater than that of the baseline configuration. Although this joint is more stiff in bending, it possesses a simpler topology, is much more rigid in compression, and the movement

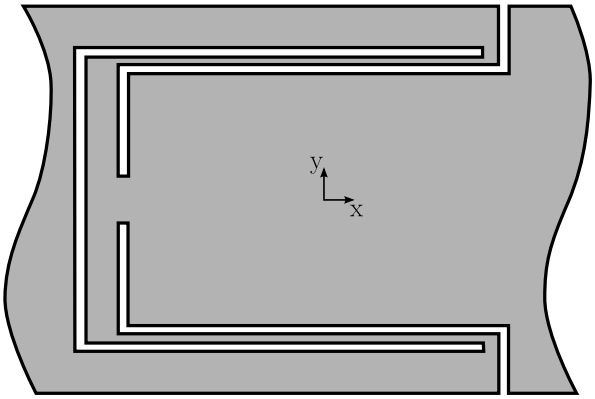

Figure 3.10: Alternative configuration of the I-LET joint

of the center of rotation is slightly less than that of the baseline configuration; the center of rotation moves a total of 0.326 mm in the $-x$ direction, or 0.65% of the joint length.

3.3 The Tension LET (T-LET) Joint

The I-LET joint is well suited for compressive loads, but is not well suited for tensile loading. The Tension LET (T-LET) joint, shown in Figure 3.11 with its accompanying linear spring model, is designed to bear in-plane tensile loads (in the positive x direction) with very little deflection. It can be viewed as a LET joint modified with long tension "straps" that deflect easily in bending, but are rigid under tension loads. Using the same methodology as before, the T-LET joint was optimized for minimum bending stiffness. Also as before, the joint was constrained to 50 mm by 50 mm area.

3.3.1 Closed-Form Model

Closed-form equations were developed to be used for the geometry optimization. The dimensions labels are shown in Figure 3.12. The bending stiffness, $k_{eq,bend}$, is

$$k_{eq,bend} = \frac{2k_{bl}k_{tl}k_{cl}}{4k_{bl}k_{tl} + k_{cl}(2k_b l + k_{tl})} + 2k_{te} \tag{3.15}$$

where,

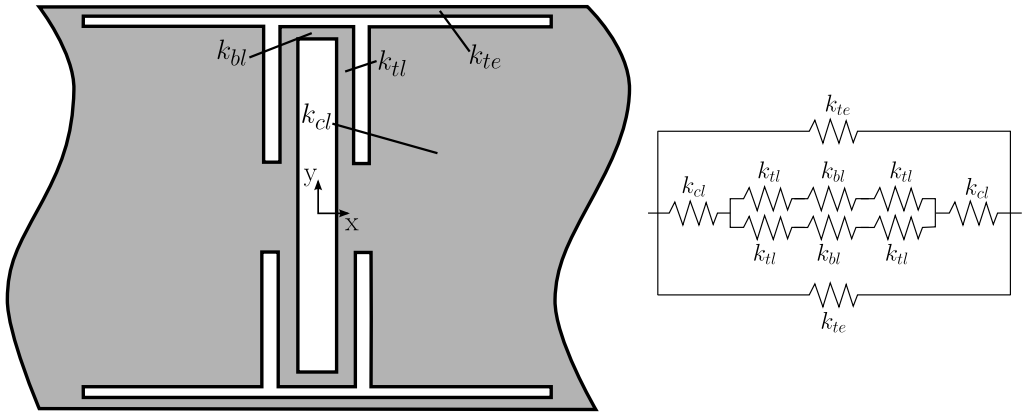

(a) The T-LET joint (b) Linear spring model

Figure 3.11: Tension LET (T-LET) joint and its associated linear spring model

$$k_{bl} = \frac{Ew_{bl}t^3}{12l_{bl}} \tag{3.16}$$

$$k_{tl} = w_{tl}t^3\frac{G}{l_{tl}}\left[\frac{1}{3} - 0.21\frac{t}{w_{tl}}\left(1 - \frac{t^4}{12w_{tl}}\right)\right] \tag{3.17}$$

and

$$k_{cl} = \frac{Ew_{cl}t^3}{12l_{cl}} \tag{3.18}$$

$$k_{te} = \frac{Ew_{te}t^3}{12l_{te}} \tag{3.19}$$

$$\tag{3.20}$$

The tensile stiffness $k_{eq,tens}$, can be determined as

$$k_{eq,tens} = \frac{k_{cl,a}k_{tl,a}}{2k_{tl,a} + k_{cl,a}} + 2k_{te,a} \tag{3.21}$$

where

$$k_{cl,a} = \frac{w_{cl}tE}{l_{cl}} \tag{3.22}$$

$$k_{tl_a} = \frac{Etw_{tl}^3}{l_{tl}^3} \tag{3.23}$$

$$k_{te,a} = \frac{w_{te}tE}{l_{te}} \tag{3.24}$$

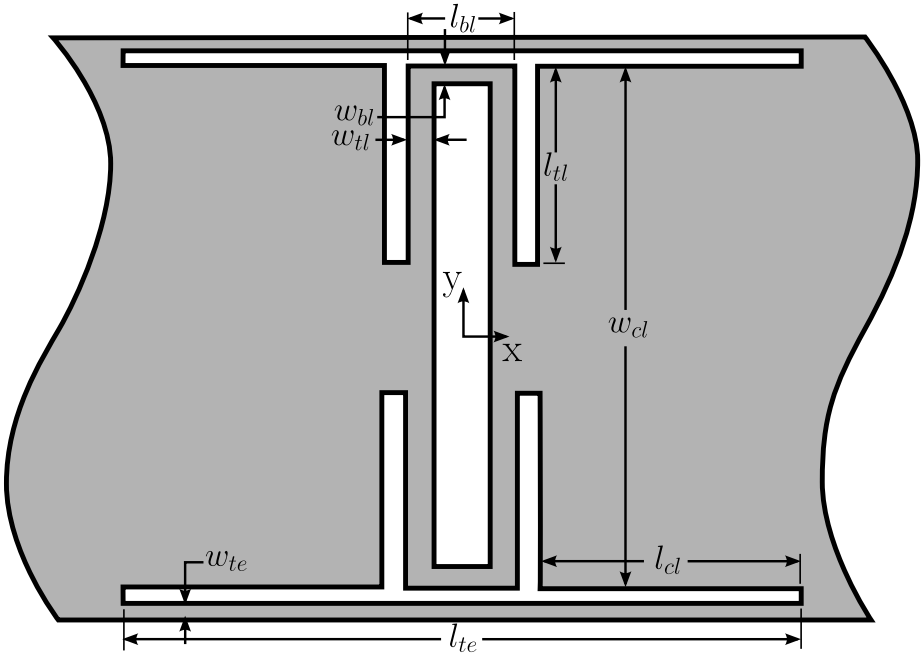

Figure 3.12: Dimension labels for the T-LET joint

3.3.2 FEA Model

The dimensions obtained from the optimization are listed in Table 3.4. As with the I-LET joint, a LET joint was optimized for axial tensile stiffness, while maintaining the same bending stiffness as the T-LET joint. The dimensions of the optimized LET joint are listed in Table 3.5. Two FEA models were created for the T-LET joint: one for bending and one for tension. In Figure 3.13, it can be seen that the FEA model is made up of two separate entities (the main body of

the joint, and the tension strap), with only boundary conditions coupling the two entities. The bending model used additional beam elements to properly couple the free ends of the two entities. These beam elements were made sufficiently rigid so that they did not significantly contribute to the deflection of the joint. The FEA model used for tension did not require the additional elements. The model used for bending contained 5353 elements. The model used for tension contained 5250 elements. The benchmark LET joint contained 946 elements. As with the I-LET joint, the FEA model of the T-LET joint was fixed at one end and displaced 30° about the y axis on the other to determine the bending stiffness, and 0.2 mm in the x to determine the tensile stiffness.

Table 3.4: Dimensions of the T-LET joint optimized for minimum bending stiffness

Dimension	Value (mm)	Dimension	Value (mm)
l_{bl}	4	l_{cl}	22
w_{bl}	1	w_{cl}	46
l_{tl}	20	l_{te}	50
w_{tl}	1	w_{te}	1
t	1		

Table 3.5: Dimensions of a LET joint optimized for a bending stiffness equivalent to the T-LET joint and maximum tensile stiffness

Dimension	Value (mm)
l_{bl}	4
w_{bl}	1
l_{tl}	7.046
w_{tl}	1
t	1

An image of the FEA bending model of the T-LET joint in its deflected position is shown in Figure 3.13. The results of the FEA modeling are summarized in Table 3.6. It can be seen in Figure 3.13 that the torsion members of the joint are not being deflected by pure torsion, which results in a nonlinear moment/deflection curve, which is shown in Figure 3.14. A trend line is also shown in this plot, with an R^2 value of 0.9967, indicating that the curve is nearly linear. The value reported for the finite element $k_{eq,bend}$ in Table 3.6 is the slope of the trend line.

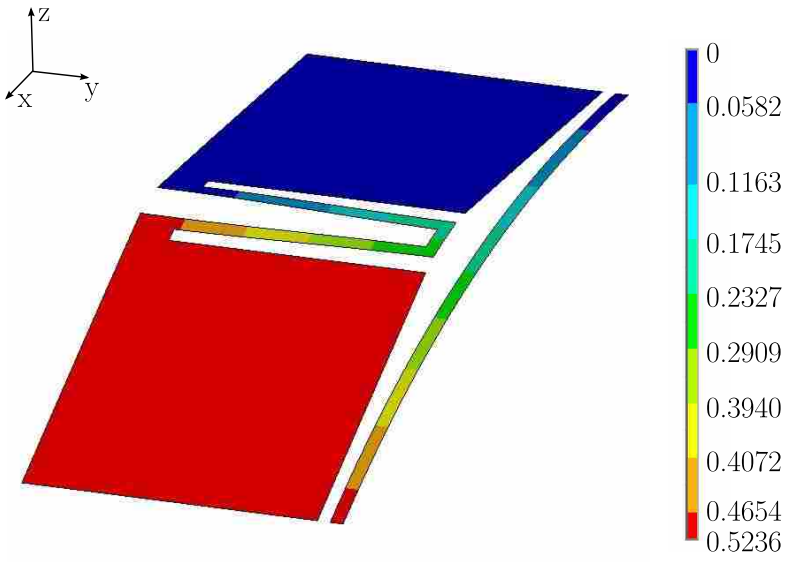

Figure 3.13: FEA model of the T-LET joint showing the deflected position in bending, indicating rotation about the *y* axis

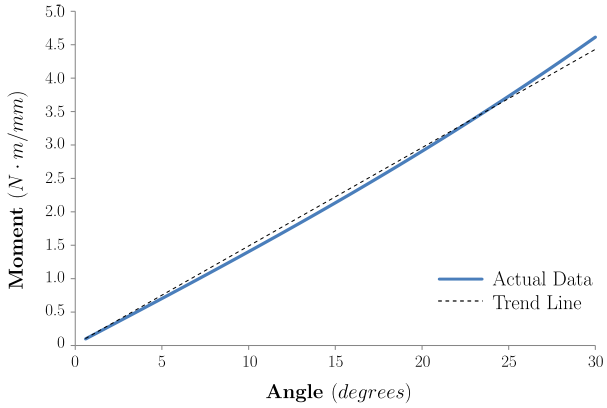

Figure 3.14: Moment/deflection curve for the T-LET joint

As shown in Table 3.6, the T-LET joint is 21 times more stiff than the optimized LET joint when subjected to an in-plane tensile load. The T-LET joint takes up more area than the LET joint, and has a slightly more complex topology, although it is still simple. It does not effectively carry compressive loads due to buckling of the tension straps. Since the joint is symmetric about the *y* axis, determining the center of rotation of the joint can be easily determined by visual inspection

so a figure indicating the center of rotation will not be provided. The center of rotation does move slightly throughout the bending motion of the joint. This is shown in Figure 3.15. The center of rotation moves a total of 0.57 mm for a 30° rotation of the joint. This represents 1.1% of the total length of the joint.

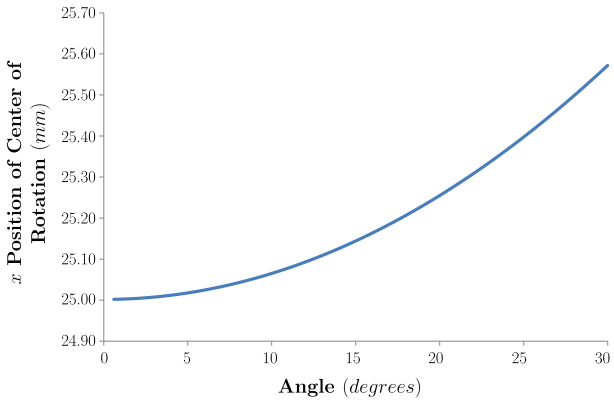

Figure 3.15: x position of the center of rotation of the T-LET joint

Table 3.6: Comparison of joint stiffnesses: T-LET and LET joints

	T-LET Joint	LET Joint	Ratio
$k_{eq,bend}(N \cdot mm/rad)$	8.428	8.896	0.95
$k_{eq,tens}(N/m)$	55750	2653	21.01

3.4 The Inverted Tension LET (IT-LET) Joint

The Inverted Tension LET (IT-LET) joint is a combination of the I-LET and T-LET joints, and is capable of effectively bearing compressive and tensile loads with minimal deflection. Closed-form equations of the IT-LET were not developed, due to the complexity of the interactions of the different joint components. A schematic of the joint is shown in Figure 3.16.

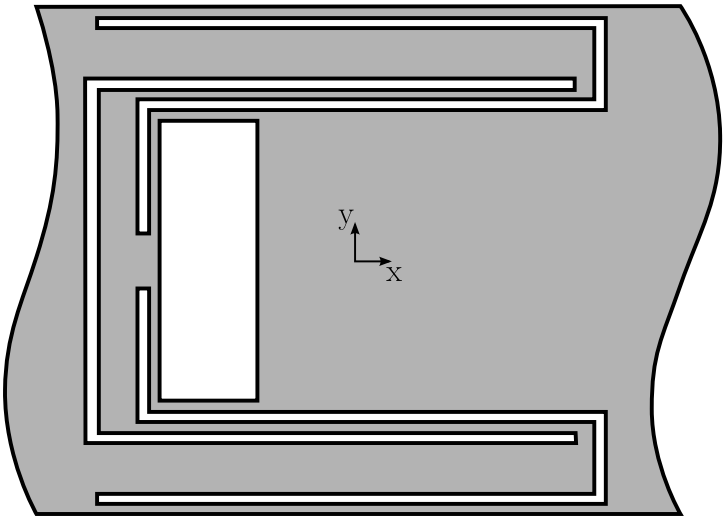

Figure 3.16: Schematic of the Inverted-Tension LET (IT-LET) joint

3.4.1 FEA Model

Using the dimension of the optimized I-LET and T-LET joints, an FEA model of the joint was created. The dimensions are summarized in Table 3.7. As discussed in Section 3.2.1, the total width of the joint is 50 mm. The labels are the same as those used for the I-LET joint, and as with the T-LET, l_{te} and w_{te} represent the length and width, respectively, of the tensions straps. As with the other joints, a LET joint was optimized for maximum axial stiffness, while maintaining the same bending stiffness as the optimized IT-LET. The dimensions are summarized in Table 3.8.

Table 3.7: Dimensions of the IT-LET joint optimized for minimum bending stiffness

Dimension	Value (mm)	Dimension	Value (mm)
l_{b1}	8	l_{t1}	12
w_{b1}	1	w_{t1}	1
l_{b2}	43	l_{t2}	14
w_{b2}	1	w_{t2}	4
l_{b3}	47	l_{t3}	7
w_{b3}	5	w_{t3}	2
l_{b4}	36	l_{te}	7
w_{b4}	30	w_{te}	2
t	1		

Table 3.8: Dimensions of the LET joint optimized for a bending stiffness equivalent to the IT-LET joint and maximum compressive and tensile stiffnesses

Dimension	Value (mm)
l_{bl}	4.291
w_{bl}	1
l_{tl}	5
w_{tl}	1.131
t	1

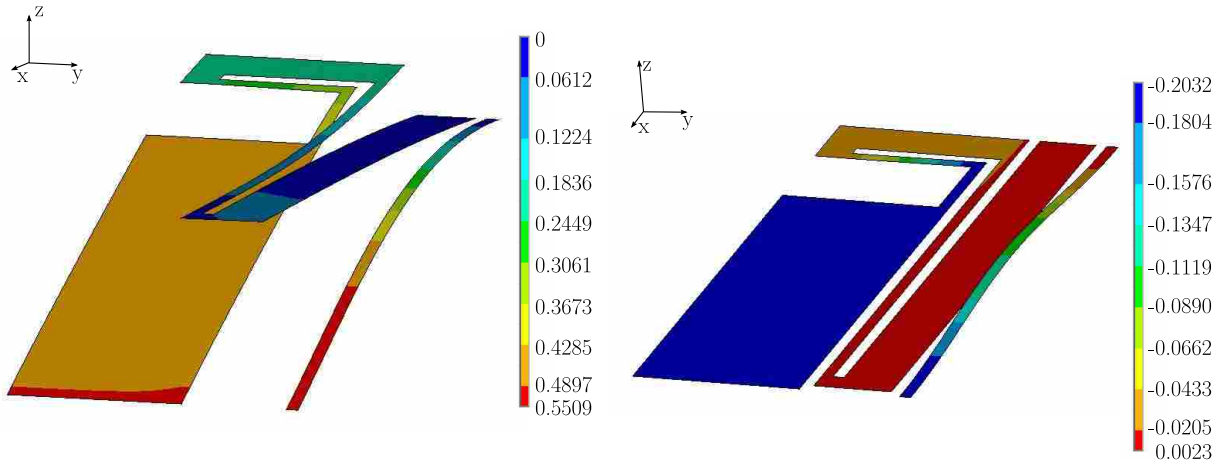

(a) FEA model of the IT-LET joint showing the deflected position in bending, indicating rotation about the y axis

(b) FEA model of the IT-LET joint showing the deflected position in compression, indicating translation along the x axis

Figure 3.17: Deflected positions of IT-LET joint FEA models

Figure 3.17 shows the deflected FEA models of the IT-LET in bending and compression. Tension is not shown since the visualization offers little additional information. Notice that in compression, the tension straps buckle and do little to bear the compressive load. As with the T-LET joint, two FEA models were required for the IT-LET joint: one for bending, and the other for tension and compression. The model used for bending included additional beam elements to ensure that the free end of the model was properly coupled; it contained 9804 elements. The model used for tension and compression contained 9743 elements. The benchmark LET joint contained 869 elements. The results of the FEA are summarized in Table 3.9. As with the T-LET joint, the IT-LET joint has a nonlinear moment deflection curve, which is shown in Figure 3.18. A trend line is also shown which has an R^2 value of 0.9712. The slope of this line is the reported FEA

bending stiffness value in Table 3.9. The IT-LET joint is 6.99 times stiffer in compression then the benchmark LET joint and 7.13 times stiffer in tension.

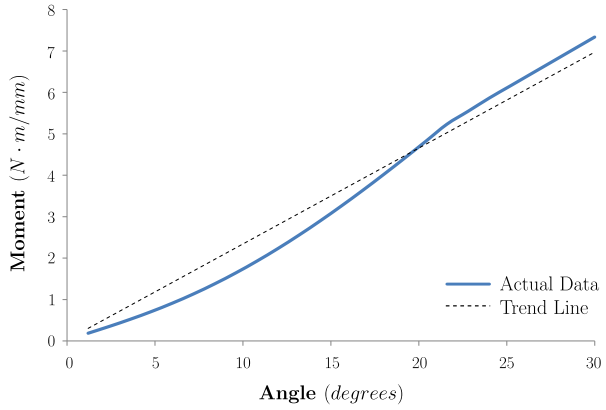

Figure 3.18: Moment/deflection curve for the IT-LET joint

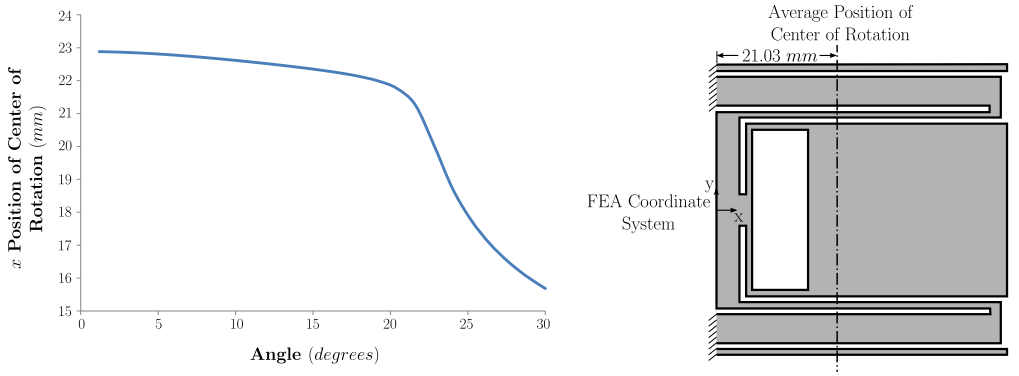

(a) x position of the center of rotation of the IT-LET joint

(b) Average position of the center of rotation of the IT-LET joint for a 30° rotation

Figure 3.19: Determining the center of rotation of the IT-LET joint

This joint has the same disadvantages as the previous joint, in that it takes up more area than the LET joint. The movement of the center of rotation is another concern. As discussed with the T-LET, adding tension straps to the I-LET joint modifies the motion path of the end of the joint. The position of the center of rotation is found the same way as was used for the I-LET and

Table 3.9: Comparison of joint stiffnesses: IT-LET and LET joints

	IT-LET Joint	LET Joint	Ratio
$k_{eq,bend}(N \cdot mm/rad)$	13260	14395	0.92
$k_{eq,comp}(N/m)$	54960	7865	6.99
$k_{eq,tens}(N/m)$	56690	7945	7.13

the results are plotted in Figure 3.19(a). Through the 30° motion of the joint, the center of rotation moves 7.2 mm, or 14.4% of the length of the joint. It is recommended that additional work be done to attempt to minimize the movement of the center of rotation for this joint. The average position of the center of rotation of this joint is located 21.03 mm from the fixed end of the joint in the FEA model's coordinate system (indicated in Figure 3.19(b)).

3.5 Applications

To demonstrate the joints as a part of various LEM mechanisms, a LEM four-bar was made using the IT-LET joint as shown in Figure 3.20. A multi-layer [6] spherical mechanism was made using the I-LET joint as shown in Figure 3.21. These two applications showed the joint's compatibility with these LEM mechanisms. If a mechanism like the crank-slider shown in [26], which is actuated with a compressive force, used the I-LET joint, the analysis could be simplified since the joints could minimize the parasitic motion in the mechanism. Other LEM applications that require tension and compression loads for actuation would benefit from the implementation of the I-LET, the T-LET, and the IT-LET joints. Many such applications are shown in [6].

3.6 Conclusions

Three LEM joints were introduced: the I-LET, the T-LET, and the IT-LET. The joints demonstrate an ability to reduce parasitic motion in LEMs when subjected to in-plane tension and/or compression loads. The applicable loading conditions for each joint, as well as important joint characteristics are summarized in Table 3.10, including the movement of the center of rotation, non-linearity of the moment-deflection curve, and the area required by the joint. Along with the LET joint, these joints offer a wide variety of capabilities for LEM joints.

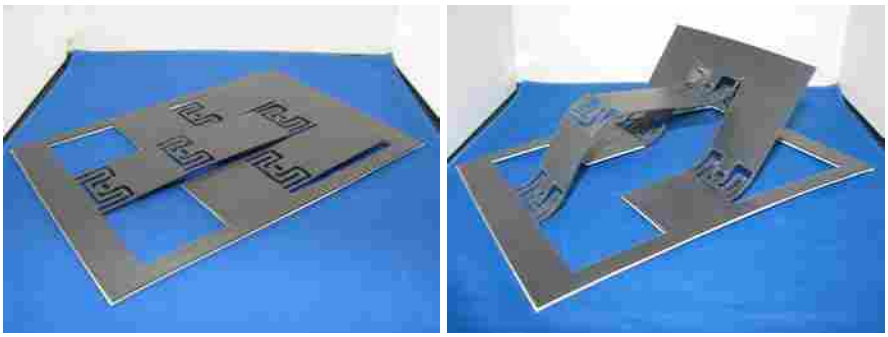

(a) 4R linkage in planar position (b) 4R linkage in actuated position

Figure 3.20: 4R linkage with IT-LET joints

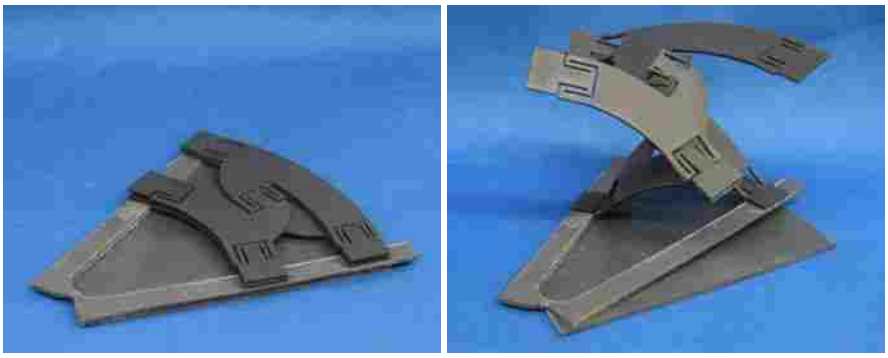

(a) Multi-layer spherical LEM in planar position (b) Multi-layer spherical LEM in actuated position

Figure 3.21: Multi-layer spherical LEM with I-LET joints

While the joints tend to take up more area than LET joints with equivalent bending stiffnesses, they demonstrate higher stiffness in compressive and/or tensile loading loading conditions. LEMs that require tension or compression loads for actuation is existing are of LEM applications

Table 3.10: Summary of relative joint performance

	Relative Off-axis Stiffness		**Performance Considerations**	
	Compression	Tension	Non-linear Moment-Deflection Curve	Area
LET	Benchmark	Benchmark	No	Benchmark
I-LET	Better	Worse	No	Worse
T-LET	Same	Better	Yes	Worse
IT-LET	Better	Better	Yes	Worse

that would benefit from the use of these joints. Many of the multi-layer LEMs developed in [6] use this form of actuation. Additionally, this group of joints broadens the options available to engineers developing lamina emergent mechanism applications.

CHAPTER 4. LEM APPLICATIONS: THE LENS LIFT™ [1]

The Lens Lift™ is a lamina emergent mechanism (LEM) that improves sterility and ease of use of contact lenses. Upon opening a contact lens container (such as a blister pack), the Lens Lift™ mechanism is actuated and it presents the contact lens to the user in an orientation that requires only one touch-point on the eye-lid (the side that does not come into contact with the eye) side of the lens to insert into the eye. A prototype Lens Lift™ was designed and constructed to be compatible with current blister pack design without making radical changes to the manufacturing process. The concepts also apply to other lens containers.

According to IBISWorld, nearly 50% of opthalmic industry is associated with contact lenses. This market is expected to grow over the next five years [36]. As the market grows, educating users about the proper use and care of contact lenses becomes increasingly important. Keeping contact lenses clean is one of the most important measures users can take to protect their eyesight [37]. The Lens Lift™ minimizes the risk of germ entry into the eye by presenting the user with the contact lens in an orientation that only requires one touch-point (on the lid side of the lens) to insert into the eye.

4.1 Background

The Lens Lift™ is a novel lamina emergent mechanism. Lamina emergent mechanisms (LEMs) are a subset of compliant mechanisms [11] made from planar materials (lamina) with motion that emerges out of the fabrication plane [2]. As compliant mechanisms, they use the deflection of flexible members to achieve the desired motion. LEMs can provide feasible, repeatable solutions to advance the design and manufacturing of products. The advantages of LEMs are reducing the number of parts, reducing cost, reducing weight, improving recyclability, increasing precision, and eliminating assembly [2]. These mechanisms can provide opportunities for more

[1] The contents of this chapter have been filed as a part of a provisional patent application with the U.S. Patent and Trademark Office

cost effective, compact, easy to assemble, modular products. Since LEMs are manufactured out of sheet (lamina) material, they are highly compact and lend themselves to simple manufacturing processes. Other possible applications of LEMs are shown in [3].

A demonstrative Lens Lift™ was designed for disposable contact lens blister packs. An example of a blister pack is shown in Figure 4.1. The blister pack holds the saline solution which keeps the contact lens moist. It is heat sealed for sterility. The Lens Lift™ is designed to be compatible with the sealing process and allow for the lens to remain in solution until opened. Although this prototype is described in detail here, the concepts also apply to other lens container types.

Figure 4.1: An example of a contact lens blister pack

4.2 Design Considerations

The main criteria for selecting a concept for the Lens Lift™ were compatibility with the blister pack (including interference with mechanism motion, space constraints, and manufacturing), human variability (such that the Lens Lift™ is compatible with a range of finger sizes) and actuation (the source of energy to lift the lens, either through energy storage, user activation, or other method).

The most critical human factor was index finger thickness approximately 10 mm from the tip of the finger, since this is generally the area of the finger the lens is placed on as the lens is

put in the eye. According to [37], proper insertion of the contact lens involves placing it near the tip of the index finger, and then placing the lens in the eye. Consequently, the Lens Lift™ should lift the lens high enough for a finger to be inserted underneath it, i.e, the clearance between the bottom of the blister pack and the lens (designated h_c in Figure 4.2) must be larger than the user's finger thickness. An average finger thickness of approximately 14 mm was assumed for this design. Another important clearance parameter is the distance from the front of the blister pack bowl to the location of the lens (designated d_c in Figure 4.2), because the finger must pass through this to gain access to the underside of the lens.

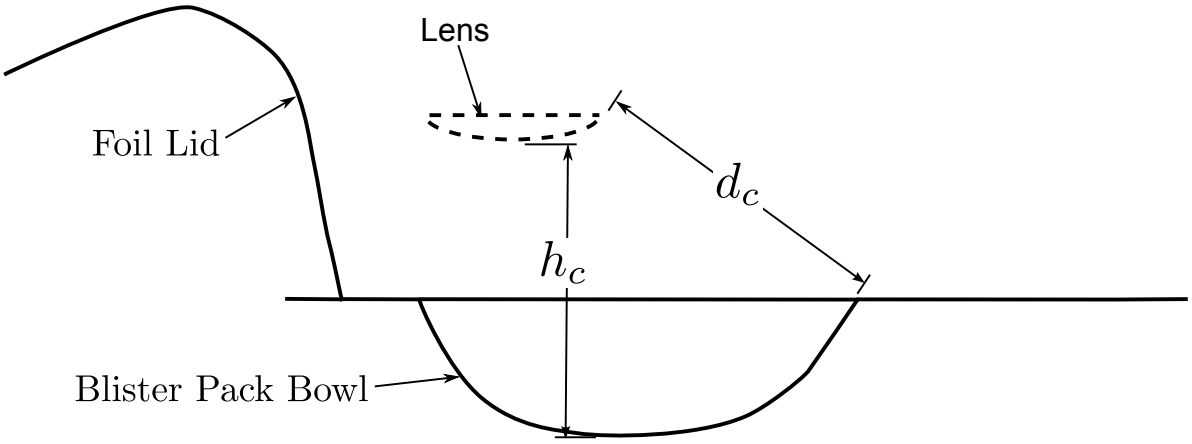

Figure 4.2: Schematic of the Lens Lift™ illustrating key clearances

Multiple concepts were explored in the design of the Lens Lift™. Some of the prototypes of these concepts are shown in Figure 4.3. Each concept improved upon the previous one in its compatibility with the actuation method and the blister pack geometry. The design of the portion of the mechanism that holds the lens, termed the cradle, was also evaluated with each concept to ensure the lens was properly supported. The concept described in detail in this work is the result of detailed analysis, multiple design iterations, and focus groups. The earliest designs were not monolithic and required multiple layers. For simplified manufacturing and assembly, it was desired to create the mechanism from a single, monolithic layer. LEMs with multiple layers are further discussed in [6].

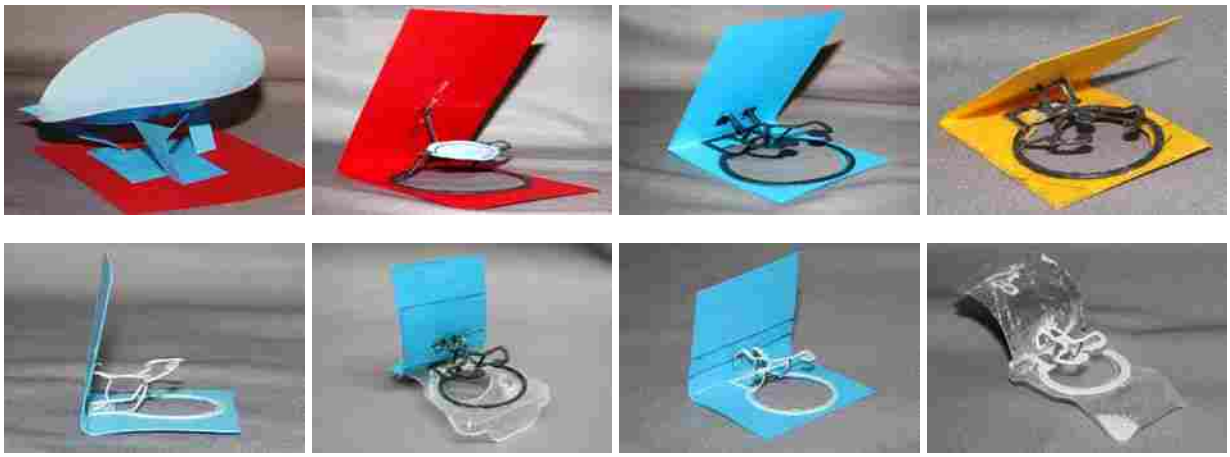

Figure 4.3: Various prototypes that were created in the development of the Lens Lift™

4.3 Synthesis

The desired Lens Lift™ motion path is translation without rotation, without interference with the container geometry, and enough clearance with the blister pack to allow a finger to be inserted under the lens. These constraints led to a concept involving a parallel-guiding mechanism, because it allows the coupler link to remain parallel to the ground link throughout the entire motion of the mechanism.

The motion of opening the blister pack lid was chosen as the most preferred actuation method for the mechanism, which required the parallel guiding mechanism to be linked to the lid with the following criteria: the lens needed to be inside the blister pack bowl when the lid was closed, thus submerged in the saline solution; when the lid was completely open, the lens needed to be lifted to a height that allowed easy access to the lens. This is illustrated in Figure 4.4.

A challenge of working with LEMs is a limited availability of joint types [7]. The joints are limited by thickness of the material used. Also, when working with compliant mechanisms, a commonly cited advantage is the energy stored in the flexible members when they are deflected. In this case energy storage was undesirable. Since the mechanism is a LEM, its neutral position is completely flat (in line with the plane of fabrication), meaning that any stored energy would be "pushing" the mechanism back to its planar position. It was desired to have the blister pack stay open once it had been opened, so that the mechanism did not have to be held in place by the user

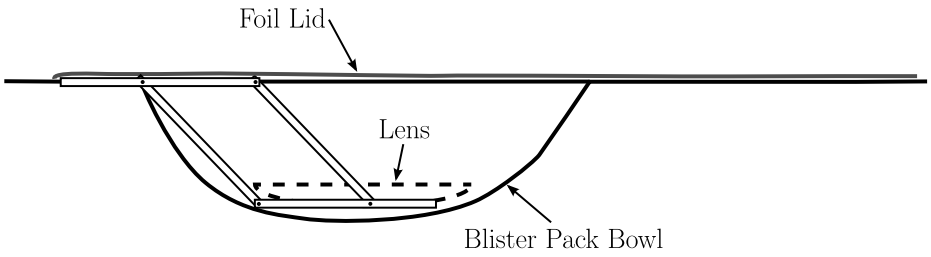

(a) Desired mechanism position when blister pack is closed

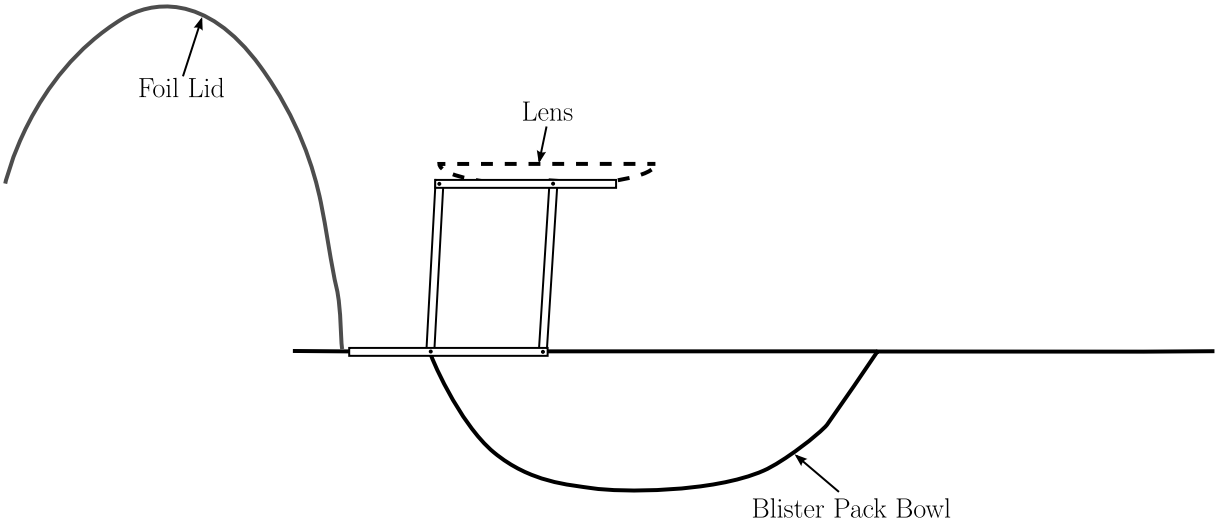

(b) Desired mechanism position when blister pack is open

Figure 4.4: Desired closed and opened positions of the mechanism

while the lens was accessed. For minimal energy storage, living hinges [11] were chosen as the compliant joint type.

A kinematic model of the mechanism is shown in Figure 4.5. It is made up of a driving linkage, where r_{d2} is formed by the lid of the blister pack, and a parallel guiding mechanism. The link r_{d3} connects the parallel guiding mechanism to the lid. These links form the driver dyad for the Lens Lift™.

With θ_{d2} as the input, θ_{d3} and θ_2 are defined by

$$\theta_{d3} = \psi_d - \beta_d \tag{4.1}$$

$$\theta_2 = \pi - \lambda_d - \beta_d \tag{4.2}$$

where

$$\delta_d = (r_{d1}^2 + r_{d2}^2 - 2r_{d1}r_{d2}\cos\theta_{d2})^{1/2} \tag{4.3}$$

$$\beta_d = \cos^{-1}\frac{r_{d1}^2 + \delta_d^2 - r_{d2}^2}{2r_{d1}\delta_d} \tag{4.4}$$

$$\psi_d = \cos^{-1}\frac{r_{d3}^2 + \delta_d^2 - r_d^2}{2r_{d3}\delta_d} \tag{4.5}$$

$$\lambda_d = \cos^{-1}\frac{r_2^2 + \delta_d^2 - r_{d3}^2}{2r_2\delta_d} \tag{4.6}$$

The y position of the cradle, y_c is related to the input angle θ_{2d} by the following equation

$$y_c = r_2\sin(\pi - \lambda_d - \beta_d) \tag{4.7}$$

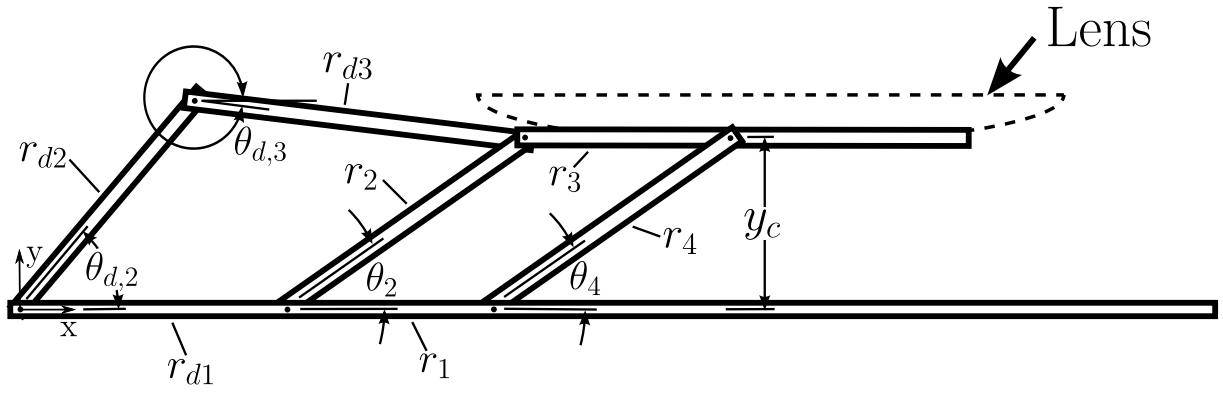

Figure 4.5: Kinematic model of the Lens Lift™ Mechanism

4.3.1 Force Relationships

The applied forces and stiffnesses associated with compliant joints are shown in Figure 4.6. The stiffnesses k_4 and k_5 appear on the same joint, but refer to two different stiffnesses. k_4 is associated with the movement of link r_{d3} relative to link r_3. k_5 is associated with the movement of link r_2 relative to r_3. These are the stiffnesses associated with the compliant joints of the mechanism.

F_l represents the weight that can be lifted for a given input force. t is a constant between 0 and 1 that determines how F_l is distributed to the links r_2 and r_4. F_i is the input force at some arbitrary orientation defined by

$$F_i = F_{i,x}\hat{i} + F_{i,y}\hat{j} \tag{4.8}$$

where $F_{i,x}$ and $F_{i,y}$ are the components of F_i in the x and y directions, respectively.

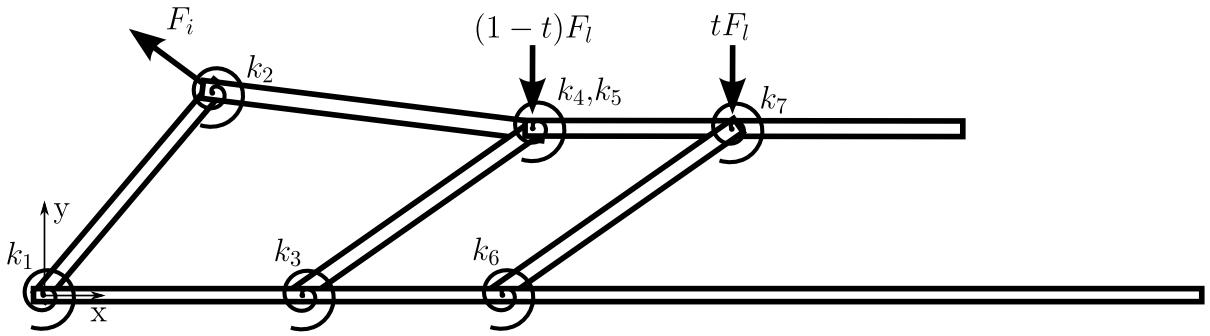

Figure 4.6: Applied forces and joint stiffness of the Lens Lift™

The kinematic coefficients $h_{d3,d2}$, $h_{2,d2}$ and $h_{4,d2}$ will be used in the virtual work analysis and are defined in Equations (4.9) through (4.9).

$$
\begin{aligned}
h_{d3,d2} &= \frac{d\theta_{d3}}{d\theta_{d2}} \\
&= \frac{r_{d2}\sin(\theta_2 - \theta_{d2})}{r_{d3}\sin(\theta_{d3} - \theta_2)} \\
h_{2,d2} &= \frac{d\theta_2}{d\theta_{d2}} \\
&= \frac{r_{d2}\sin(\theta_{d3} - \theta_{d2})}{r_2\sin(\theta_{d3} - \theta_2)}
\end{aligned}
$$

Using Equations (4.1) through (4.6), the kinematic coefficients become

$$
h_{d3,d2} = \frac{r_{d2}\sin(\pi - \lambda_d - \beta_d - \theta_{d2})}{r_{d3}\sin(\psi_d - \lambda_d - 2\beta_d - \pi)} \tag{4.9}
$$

$$
h_{2,d2} = \frac{r_{d2}\sin(\psi_d - \beta_d)}{r_2\sin(\psi_d - \lambda_d - 2\beta_d - \pi)} \tag{4.10}
$$

Recall that $\theta_4 = \theta_2$, thus

$$
h_{4,d2} = h_{2,d2} \tag{4.11}
$$

Using the kinematic coefficients defined in Equations (4.9) through (4.10), the virtual work for this system is

$$
\begin{aligned}
\delta W = [&r_{d2}(-F_{i,x}\sin\theta_{d2} + F_{i,y}\sin\theta_{d2}) - F_l(r_{d1} + r_2\cos\theta_2(1-t) + t(r_1 + r_4\cos\theta_4)) \\
&- k_1\Delta\theta_{d2} + k_2(\Delta\theta_{d2} - \Delta\theta_{d3})h_{d3,d2} - k_3\Delta\theta_2 h_{2,d2} - k_4\Delta\theta_{d3}h_{d3,d2} \\
&- k_5\Delta\theta_2 h_{2,d2} - k_6\Delta\theta_4 h_{4,d2} - k_7\Delta\theta_4 h_{4,d2}]\delta\theta_{d2}
\end{aligned} \tag{4.12}
$$

Since $r_2 = r_4$, $\theta_4 = \theta_2$, and from Equation (4.11), Equation (4.12) simplifies to

$$\delta W = [r_{d2}(-F_{i,x}\sin\theta_{d2} + F_{i,y}\cos\theta_{d2}) - F_l(r_{d1} + r_2\cos\theta_2 + tr_1) - k_1\Delta\theta_{d2} + (k_2\Delta\theta_{d2} - (k_2+k_4)\Delta\theta_{d3})h_{d3,d2} - (k_3+k_5+k_6+k_7)\Delta\theta_2 h_{2,d2}]\delta\theta_{d2} \quad (4.13)$$

Assuming the input force is always directed tangent to link r_{d2}

$$F_{i,x} = F_i\sin\theta_{d2} \quad (4.14)$$

$$F_{i,y} = F_i\cos\theta_{d2} \quad (4.15)$$

where F_i is the magnitude of the input force. Also, since the initial position of all the links is in line with the fabrication plane the undeflected (or initial) angle for each link is zero. Thus

$$\Delta\theta_{d2} = \theta_{d2} \quad (4.16)$$

$$\Delta\theta_{d3} = \theta_{d3} \quad (4.17)$$

$$\Delta\theta_2 = \theta_2 \quad (4.18)$$

Assuming the mechanism is in equilibrium, $\delta W = 0$. A relationship for the force required to actuate the mechanism for a given input angle can now be developed. Note that this actuation force refers to the mechanism actuation only, and not the force required to undo the heat seal of the blister pack. Using Equations (4.1) through (4.6), and (4.14) through (4.18), the input force for a given θ_{d2} can be found and is shown below

$$F_i = \left(\frac{1}{r_{d2}(2\cos^2\theta_{d2} - 1)}\right)[F_l(r_{d1} + r_2\cos(\pi - \lambda_d - \beta_d) + tr_1) + k_1\theta_{d2} - (k_2\theta_{d2} + (k_2+k_4)(\psi_d - \beta_d))h_{d3,d2} + (k_3+k_5+k_6+k_7)(\pi - \lambda_d - \beta_d)h_{2,d2}] \quad (4.19)$$

4.4 Prototype

A prototype of the Lens Lift™ was built using the link lengths shown in Table 4.1. Using Equations (4.1) through (4.6), the motion path of the prototype was determined. The opened and

closed positions of the prototype are shown in Figure 4.7 and they fulfill the design objectives discussed in Section 4.3. Note that for simplicity the cradle is not shown in Figure 4.7 but is shown in Figure 4.8. Using Equation 4.7, in the closed position $y_c = -6.08$mm. Assuming $\theta_{d2} = 110^o$ in the open position, $y_c = 8$mm. The blister pack depth of the prototype is approximately 7 mm, thus $h_c = 15$ mm (see Figure 4.2). The prototype also achieves a d_c clearance of approximately 15 mm. These values both exceed the assumed finger thickness, and thus a finger of the assumed thickness will have convenient access to the lens. The clearance values are largely limited by the blister pack geometry. Slight modifications to the blister pack could result in greater clearances.

Table 4.1: Prototype link lengths

Dyad Four-bar		Parallel Four-bar	
Link	Length	Link	Length
r_{d1}	3.5 mm	r_1	4 mm
r_{d2}	7.5 mm	r_2	8 mm
r_{d3}	6.2 mm	r_3	4 mm
r_{d4}	8 mm	r_4	8 mm

A schematic of the prototype is shown in Figure 4.8. This figure does not include link r_{d2} since that link is formed by the lid, which is not shown. The lid attachment pads are the areas that allow the mechanism to be attached to the foil lid of the blister pack. Axis A denotes the point about which the lid (link r_{d2}) rotates. This axis moves throughout the opening of the blister pack as the foil lid is peeled back. However when it reaches the point shown in the figure, the lens can be easily accessed, and the lid does not need to be peeled back any further (further moving axis A). When axis A reaches the point shown in Figure 4.8, it is assumed that it does not move further and that the only motion of the lid is rotation about A. The cradle was designed to support the lens throughout the motion of the mechanism and to allow a finger to easily pass through the members as the lens is picked up. It is also designed to conform to the surface of the blister pack bowl when the Lens Lift™ is in its closed position, effectively "cupping" lens so that it remains on the cradle at all times while the blister pack is sealed closed.

The prototype is shown in Figure 4.9. The mechanism was laser cut from a single layer of PTFE. Figure 4.9(a) shows the mechanism as cut by the laser cutter. The living hinges were created

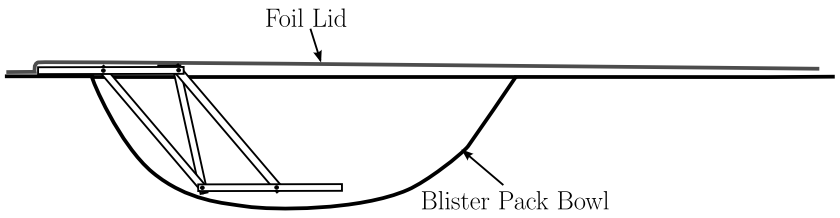

(a) Closed Position

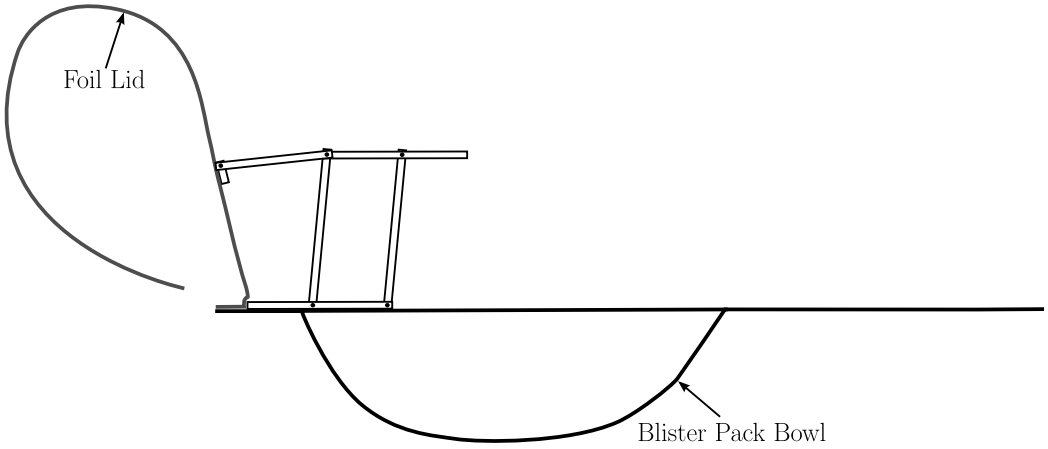

(b) Open Position

Figure 4.7: Closed and open positions of the Lens Lift™ prototype illustrating the motion path

by scoring the PTFE at the joint locations, shown in Figure 4.8. Fatigue life is not a concern in this design since only one cycle is required. The scored joints were sufficient for verification of the design. Each joint can be assumed to have the same stiffness (except for stiffness k_1, since this joint is formed by the foil lid, not a living hinge). Let k_{lh} be the stiffness of each living hinge and k_{fl} be the stiffness of joint formed by the foil lid. The stiffnesses of each of the joints shown in Figure 4.6 become

$$k_1 = k_{fl} \tag{4.20}$$

$$k_2 = 2k_{lh} \tag{4.21}$$

$$k_3 = k_{lh} \tag{4.22}$$

$$k_4 = 2k_{lh} \tag{4.23}$$

$$k_5 = k_{lh} \tag{4.24}$$

$$k_6 = 2k_{lh} \tag{4.25}$$

$$k_7 = 2k_{lh} \tag{4.26}$$

Using Equations (4.20) through (4.26), Equation (4.19) can be simplified to

$$\begin{aligned} F_i = \left(\frac{1}{r_{d2}(2\cos^2\theta_{d2}-1)}\right)[&F_l(r_{d1}+r_2\cos(\pi-\lambda_d-\beta_d)+tr_1) \\ &-k_f l\theta_{d2}+k_{lh}(\theta_{d2}-2(\psi_d-\beta_d)h_{d3,d2}-6k_{lh}(\pi-\lambda_d-\beta_3)h_{2,d2}] \end{aligned} \tag{4.27}$$

The prototype demonstrated the functionality of the Lens Lift™ . It showed that it was compatible with the blister pack. The link lengths and cradle design can readily be modified to make the mechanism compatible with other blister pack geometries.

4.5 Conclusions

An example of an application of LEMs has been described. The Lens Lift™ is a lamina emergent mechanism that presents the contact lens to users as the blister pack is opened. The mechanism is cut from a flat sheet and possesses a monolithic structure. The kinematics of the mechanism have been described, as well as the relationship of the required input force to the input angle. A prototype was made to be compatible with available blister packs. It demonstrated its ability to achieve the desired motion and create the necessary clearances for convenient access to the lens. This prototype was built to be compatible with a particular blister pack, but the analysis applies to other designs and blister pack geometries.

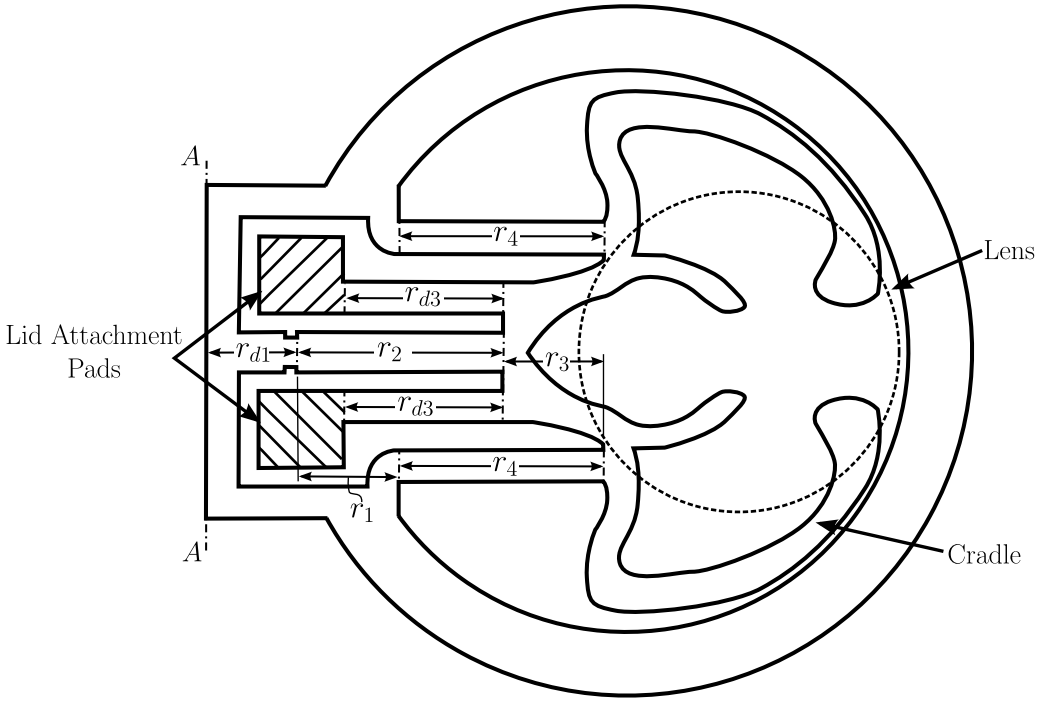

Figure 4.8: Schematic of the Lens Lift™ prototype

(a) As cutout (b) Sideview (c) Isometric view

Figure 4.9: Physical prototype of the Lens Lift™

A provisional patent has been filed with the U.S. Patent and Trademark office. Focus groups consisting of 5 to 6 individuals have evaluated prototypes and provided feedback on the Lens Lift™. A major contact lens manufacturer is currently evaluating the concept for possible inclusion in their products.

CHAPTER 5. CONCLUSIONS AND RECOMMENDATIONS

This thesis has expanded the basic understanding of LEMs and provides research that will be useful in more fully employing LEMs in applications. Spherical LEMs have been introduced, new joints have been developed, and a case study of LEMs design is provided.

5.1 Conclusions

To further investigate the capabilities of LEMs and study their fundamentals, spherical LEMS were studied and application of spherical LEMs were demonstrated. A classification of all possible spherical 4R LEMs was developed. This classification groups mechanisms based on the limits of motion of each of the spherical links. It was shown that the characteristics of 4R spherical LEMs could be used to predict motion limits of 6R spherical LEMs and arrays of spherical LEMs. Prototypes of the discussed mechanisms were created and analyzed. Multiple methods of configuring an array of spherical LEMs was also demonstrated.

Three LEM joints were introduced; the I-LET, the T-LET, and the IT-LET joint. The I-LET joint showed increased compressive stiffness over a LET joint with the same bending stiffness. The same was shown with the T-LET and the IT-LET joints, for tension and tension/compression loading respectively. The joints generally require more area then the LET joint but can be used to reduce parasitic motion in LEMs when tension and compression loading conditions are present. These joints will be especially useful in applications where a slider is used to actuate the mechanism. In this case the actuation of the mechanisms subjects it to compressive and/or tensile loads.

The Lens Lift™, a mechanism for use with disposable contact lens blister packs, is an example of a LEM application. It is monolithic and easily manufactured from sheet goods. This work presented the kinematic equations associated with the mechanism and also showed many of the prototypes created during the design process. The design was presented to multiple focus

groups and further evaluated to meet needs expressed in the focus groups. A provisional patent was filed on the Lens Lift™.

5.2 Recommendations

This work introduced arrays of spherical LEMs and several new LEM compatible joints. While the arrays discussed in this work were small, it is recommended that larger arrays be studied. Large arrays of LEMs may find application in adaptive morphing surfaces or other related fields. It is also recommended that mechanisms utilizing the joints described in this thesis be developed and analyzed. As discussed previously, multi-layer LEMs [6] that utilize sliders for mechanism actuation are applications that could benefit from the use these joints. Doing so will prove the effectiveness of the joints and further illustrate their advantages and disadvantages. Additionally, topology optimization could be used to further optimize the joints and develop new joint types. As the capability of LEMs are expanded, more potential applications will arise and more industries will be able to benefit from the advantages of LEMs.

REFERENCES

[1] Cervantes-Sánchez, J. J., and Medellín-Castillo, H. I., 2002. "A robust classification scheme for spherical 4R linkages." *Mechanism and Machine Theory,* **37**(10), Oct., pp. 1145–1163.

[2] Jacobsen, J. O., Winder, B. G., Howell, L. L., and Magleby, S. P., 2010. "Lamina emergent mechanisms and their basic elements." *Journal of Mechanisms and Robotics,* **2**(1), pp. 1–9.

[3] Albrechtsen, N. B., Magleby, S. P., and Howell, L. L., 2010. "Identifying potential applications for lamina emergent mechansism using techonology push product development." In *34th Mechanisms and Robotics Conference, presented at ASME International Design Engineering Technical Conferences and Computers and Information in Engineering Conference, IDETC/CIE2010, August 15, 2010 - August 18, 2010*.

[4] Larochelle, P., Dooley, J., Murray, A. P., and McCarthy, J. M., 1993. "SPHINX - Software for synthesizing spherical mechanisms." In *NSF Design and Manufacturing Systems Conference* Proceedings of the 1993 NSF Design and Manufacturing Systems Conference.

[5] Chiang, C. H., 1988. *Kinematics of Spherical Mechanisms*. Cambridge University Press, June.

[6] Gollnick, P. S., Magleby, S. P., and Howell, L. L., 2011. "An introduction to multi-layer lamina emergent mechanisms." *Journal of Mechanical Design* In review for publication.

[7] Jacobsen, J. O., Chen, G., Howell, L. L., and Magleby, S. P., 2009. "Lamina emergent torsional (LET) joint." *Mechanism and Machine Theory,* **44**(11), Nov., pp. 2098–2109.

[8] Winder, B. G., Magleby, S. P., and Howell, L. L., 2009. "Kinematic representations of pop-up paper mechanisms." *Journal of Mechanisms and Robotics,* **1**(2), pp. 1–10.

[9] Makhsudyan, N., Djavakhyan, R., and Arakelian, V., 2009. "Comparative analysis and synthesis of six-bar mechanisms formed by two serially connected spherical and planar four-bar linkages." *Mechanics Research Communications,* **36**(2), Mar., pp. 162–168.

[10] Winder, B. G., Magleby, S. P., and Howell, L. L., 2009. "A study of joints suitable for lamina emergent mechanisms." In *Proceedings of the ASME International Design Engineering Technical Conferences and Computers and Information in Engineering Conference, DETC 2008*, Vol. 2, ASME, pp. 339–349.

[11] Howell, L. L., 2001. *Compliant Mechanisms*. Wiley-Interscience, July.

[12] Barker, C. R., 1985. "A complete classification of planar four-bar linkages." *Mechanism and Machine Theory,* **20**(6), pp. 535–554.

[13] Svoboda, A., 1948. *Computing Mechanisms and Linkages*. MIT Radiation Laboratory Series. No. 27. McGraw-Hill.

[14] Martin, D. P., and Murray, A. P., 2002. "Developing classifications for synthesizing, refining, and animating planar mechanisms." *ASME Conference Proceedings,* **2002**(36533), Jan., pp. 1397–1403.

[15] McCarthy, J. M., 2000. *Geometric Design of Linkages*., 1 ed. Springer, Apr.

[16] Savage, M., and Hall, J., 1970. "Unique descriptions of all spherical Four-Bar linkages." *Journal of Engineering for Industry,* **92**(3), pp. 559–563.

[17] Su, H., Collins, C. L., and McCarthy, J. M., 2002. "Classification of RRSS linkages." *Mechanism and Machine Theory,* **37**(11), Nov., pp. 1413–1433.

[18] TanIk, E., and Parlaktas, V., 2011. "A new type of compliant spatial four-bar (RSSR) mechanism." *Mechanism and Machine Theory,* **46**(5), May, pp. 593–606.

[19] Medellín-Castillo, H. I., and Cervantes-Sánchez, J. J., 2005. "An improved mobility analysis for spherical 4R linkages." *Mechanism and Machine Theory,* **40**(8), Aug., pp. 931–947.

[20] Lusk, C. P., and Howell, L. L., 2008. "Components, building blocks, and demonstrations of spherical mechanisms in microelectromechanical systems." *Journal of Mechanical Design, Transactions of the ASME,* **130**(3).

[21] Hernandez, S., Bai, S., and Angeles, J., 2006. "The design of a chain of spherical stephenson mechanisms for a gearless robotic Pitch-Roll wrist." *Journal of Mechanical Design,* **128**(2), Mar., pp. 422–429.

[22] Wampler, C. W., 2004. "Displacement analysis of spherical mechanisms having three or fewer loops." *Journal of Mechanical Design,* **126**(1), Jan., pp. 93–100.

[23] Norton, R., 2007. *Design of Machinery*., 4 ed. McGraw-Hill Science/Engineering/Math, July.

[24] Lusk, C. P., and Howell, L. L., 2004. "A micro Helico-Kinematic platform via spherical crank sliders." *ASME Conference Proceedings,* **2004**(47144), Jan., pp. 131–141.

[25] Kota, S., 2001. "Compliant systems using monolithic mechanisms." *Smart Materials Bulletin,* **2001**(3), Mar., pp. 7–10.

[26] Aten, Q. T., Zirbel, S. A., Jensen, B. D., and Howell, L. L., 2011. "A numerical method for position analysis of compliant mechanisms with more degrees of freedom than inputs." *Journal of Mechanical Design,* **133**(6), June, pp. 061009–9.

[27] Trease, B. P., Moon, Y., and Kota, S., 2005. "Design of Large-Displacement compliant joints." *Journal of Mechanical Design,* **127**(4), July, pp. 788–798.

[28] Ferrell, D. B., Isaac, Y. F., Magleby, S. P., and Howell, L. L., 2011. "Development of criteria for lamina emergent mechanism flexures with specific application to metals." *Journal of Mechanical Design,* **133**(3), Mar., pp. 031009–9.

[29] Yao, W., Cannella, F., and Dai, J. S., 2011. "Automatic folding of cartons using a reconfigurable robotic system." *Robotics and Computer-Integrated Manufacturing,* **27**(3), June, pp. 604–613.

[30] Zhao, H., Bi, S., and Yu, J., 2011. "Nonlinear deformation behavior of a beam-based flexural pivot with monolithic arrangement." *Precision Engineering,* **35**(2), Apr., pp. 369–382.

[31] Pei, X., Yu, J., Zong, G., Bi, S., and Su, H., 2009. "The modeling of cartwheel flexural hinges." *Mechanism and Machine Theory,* **44**(10), Oct., pp. 1900–1909.

[32] Dai, J. S., and Jones, J. R., 1999. "Mobility in metamorphic mechanisms of Foldable/Erectable kinds." *Journal of Mechanical Design,* **121**(3), pp. 375–382.

[33] Guerinot, A. E., Magleby, S. P., Howell, L. L., and Todd, R. H., 2005. "Compliant joint design principles for high compressive load situations." *Journal of Mechanical Design,* **127**(4), July, pp. 774–781.

[34] Roark, R. J., and Young, W. C., 1975. *Formulas for stress and strain.*, 5th ed. McGraw-Hill, New York.

[35] ANSYS Inc, 2011. ANSYS®.

[36] http://www.ibisworld.com/industryus/ataglance.aspx?indid=882, 2011.

[37] http://minnesota.aoa.org/x8024.xml, 2011.